CHALMERS
UNIVERSITY OF TECHNOLOGY

Development of a measurement platform for a SAR sensor

Master thesis in Master's program in Nanotechnology

AADITYA VENKATESHA BABU BANGARU

Department of Chemistry and Chemical Engineering
CHALMERS UNIVERSITY OF TECHNOLOGY
Gothenburg, Sweden 2020

Master's thesis in Nanotechnology

Development of a measurement platform for a SAR sensor

AADITYA VENKATESHA BABU BANGARU

CHALMERS
UNIVERSITY OF TECHNOLOGY

Department of Chemistry and Chemical Engineering
Biophysical Technology Laboratory
Chalmers University of Technology
Gothenburg, Sweden 2020

Development of a measurement platform for a SAR sensor
AADITYA VENKATESHA BABU BANGARU

Supervisor: Aldo Jesorka, Department of Chemistry and Chemical Engineering
Co-supervisor: Dr. Lauri Viitala
Examiner: Aldo Jesorka, Department of Chemistry and Chemical Engineering

Master's Thesis 2020
Department of Chemistry and Chemical Engineering
Chalmers University of Technology
SE-412 96 Gothenburg
Telephone +46 31 772 1000

Cover: Measurement platform for a SAR sensor

Typeset in LaTeX
Gothenburg, Sweden 2020

Development of a measurement platform for SAR sensor
AADITYA VENKATESHA BABU BANGARU
Department of Chemistry and Chemical Engineering
Chalmers University of Technology

Abstract

Surface Acoustic Wave (SAW) sensors have found applications in research as well as in various industries, especially in the life sciences, biomedical research, and biotechnology. The biophysical technology laboratory at Chalmers has developed a new in-liquid SAW sensing concept by combining microfluidics and new SAW technology, which resulted in Surface Acoustic Resonance (SAR) sensors. In this project, we have developed a portable measurement platform which enables SAR sensors to be applied in field studies of fluids at higher temperatures. As a part of the project, we have developed and tested a new fabrication concept of mold systems for wafer-scale fabricaition of microfluidic devices. The measurement system was used to study sucrose solutions of varying viscosities (5% to 40%) at different temperatures ($25°C$ to $40°C$).

Keywords: Surface Acoustic Resonance (SAR) sensors, replica molding, viscosity, PDMS, microfluidics, viscosity-temperature studies.

Acknowledgements

I would like to thank my supervisor Dr. Aldo Jesorka for all the help and support in my work with my master thesis. He was very kind in accepting me as a master thesis student under him and he introduced me to biophysical lab in department of Chemistry and chemical engineering at Chalmers University of Technology. He has been very supportive throughout the entire period of my thesis work.

I enjoyed working under him, learning from him and the discussions with him regarding the topics I worked were beneficial and interesting. I would like to thank him for introducing me to surface acoustic wave sensors and microfluidics without which I would not have been able to learn about. I would like to thank him for teaching me all the softwares, CNC machining and many other techniques that played crucial role in shaping my thesis work.

I would like to thank my co-supervisor Dr. Lauri Viitala who was very helpful in helping me understand various topics that were essential parts of my thesis work without which my work would have been incomplete. He was very supportive and always motivated me to try out new things throughout my thesis work.

I would like to thank Dr. Kiryl Kustanovich for teaching me the fundamental concepts required in understanding my thesis work, and Dr. Helena Rodilla for designing the coplanar waveguide.

I would also like to thank Ruslan Ryskulov, Astrid Olivefors and Baharan Ali Doosti for helping me get used to the lab working conditions initially when I started my master thesis. I also thank all my colleagues who directly and indirectly helped me. I spent great time in biophysical technology lab, meeting amazing people and learning various things which will be beneficial to me, thank you very much.

I also thank my family and friends whose support and encouragement kept me motivated all the time.

Aaditya Venkatesha Babu Bangaru, Gothenburg, June 2020

Contents

List of Figures

1

Introduction

The advent of microtechnology led to the large-scale fabrication and increased utility of sensors. The number of sensors manufactured and used in commercial products is exponentially increasing. Our modern-day smartphone is one of the products, featuring advanced sensors. The number of sensors per device is also increasing rapidly with every iteration. There has been continuous research on sensing technology in search of new sensors which might replace older generations, or have new applications. One commercially successful sensor was the Quartz Crystal Microbalance (QCM).

QCM measures mass variation per unit area by measuring the change in frequency of a quartz crystal resonator. It has found applications in many fields. The success of the QCM contributed to the development of Surface Acoustic Wave (SAW) sensors, which utilize the property of piezoelectric materials to generate surface acoustic waves.

Another new research field that originated in the end of the 20th century was the field of microfluidics. Microfluidics is an interdisciplinary field of science which deals with the manipulation and controlling of fluids (in the range of microliters to picoliters) in a network of channels which are of micrometer size. This field has also seen an exponential growth since its origin. It has found applications in research as well as in industries, especially in the field of life science, biomedical science, and biotechnology.

The Biophysical Technology Laboratory at Chalmers combined microfluidics and SAW sensing technology, which led to a Surface Acoustic Wave Resonance (SAR) sensor platform for the purpose of in-liquid sensing. These sensors have been used to study antibody binding, lipid membranes and viscous fluids. These sensors are smaller, more robust and cheaper compared to QCM. The successful journey of QCM sensors from the research lab to the commercial market is an inspiration with regards to the advancement of SAR sensor technology.

In this project we developed a measuring platform, consisting of holders to accommodate and interface the sensors, a vector network analyzer (VNA), MATLAB-based measurement software for PC, a pressure pump, a temperature controller, and fluid injection valve. Two different holders were simulated and fabricated for different

measurements. Acoustic and impedance measurements were performed with one holder. Viscosity and temperature studies were carried out with the second holder that contained a thermocouple and ceramic heater. The measurement platform is modular in nature such that any new development can be incorporated with ease.

Sucrose solutions of varying concentrations were studied at different temperatures, using the temperature-controlled measuring platform and all the results were compared with literature values.

1.1 Motivation

The commercial success of QCM in the last decade has renewed the interest in finding new ways to utilize acoustic waves in previously unexplored fields. One such area of interest was the study of biological fluids at the microscale. The biophysical technology laboratory at Chalmers has recently developed a new SAR sensor, primarily in order to study fluidic interactions with biomembranes in microfluidic channels. This SAR sensing technology is related to the QCM sensing concept, but requires very only very small fluid volumes (microliters) to operate.

Accordingly, there is the need for a simple, robust and modular portable measurement plat¬form, which would accommodate and interface the microfluidic SAR sensor system during measurements which might create applications in point-of-care testing and diagnostics.

1.2 Objective

The objective of this work is to develop temperature-controlled measurement platform for a surface acoustic resonance (SAR) sensor. The platform should make senor measurements independent from stationary equipment, such as micro-manipulators and allow sample handling via a microfluidic device. Test measurements on a suitable fluid have to be performed, temperature dependence of the measurements be investigated, and the re-usability of the sensor platform should be determined.

1.3 Need for a new measurement platform

SAR sensor is a multi-parametric sensor with many potential applications. It has the ability to make an impact in liquid-solid interface sensors. The currently most limiting condition is a lack of a proper measurement platform.

1.4 Older generations of measuring platform

Before the development of the new measurement platform, there were two different measuring platforms used for measurements.

1.4.1 First generation measuring platform: Open measurement system

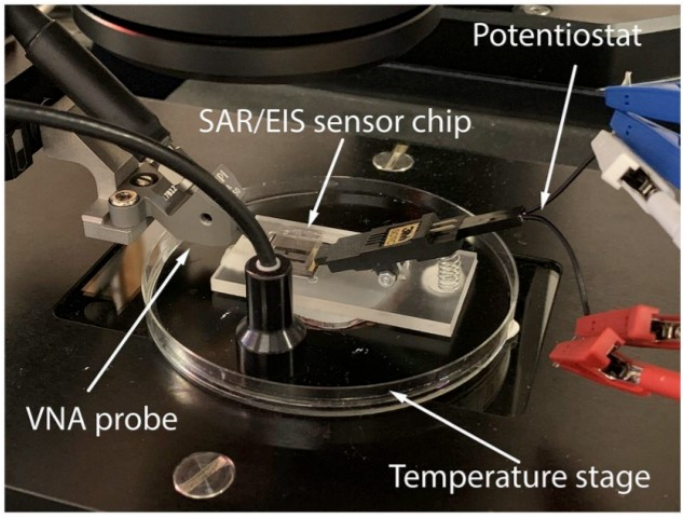

Figure 1.1: First generation measuring platform: Open measurement system using micro-manipulators for electrical interfacing [20]

This measuring platform was used during the initial stages of SAR sensor development. It involved manual injecting of fluids directly into the sensor by hand. This was a difficult injection process, as there were always the risk of injecting air bubbles and other smaller particles into the microfluidic container of the sensor. This was observed using an optical microscope. Hence, to remove unwanted bubbles or particles, multiple injection processes were required to take one measurement. The use of optical microscope also consumed some time during the injection process.

Once the injection was completed, measurements were performed in an open environment. This introduced unwanted noise and interference into the measurements.

The sensor had to be interfaced with micro-manipulators with the stationary network analyser (and potentiostat), as shown in figure 1.1. This made the measuring platform immovable and in many aspects difficult to operate. The re-usability of SAR sensor was also affected which beat the purpose of designing the sensor and that is for point-of-care testing and diagnostics. The use of micro-manipulators made the use of SAR sensor difficult, as the highly sensitive micro-probes had to be withdrawn for any operation on the sensor, such as sample change, washing, etc.

1.4.2 Second generation measuring platform: Closed system with polycarbonate sensor holder

In order to eliminate the use of micro-manipulators, and enclose the sensor, a CNC machined polycarbonate sensor holder was employed. Spring-loaded contacts connected with wires to SMA connectors were used for the electrical interfaces, and Nanoports were glued to the top part of the sensor holder for the fluid interface to the microfluidic device.

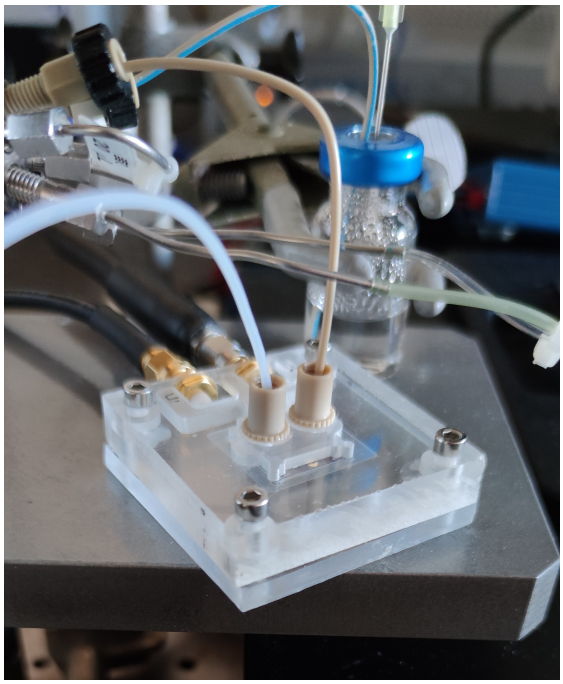

Figure 1.2: Second generation measuring platform: Closed system with polycarbonate sensor holder, Nanoports as fluid inlets, and SMA connectors

The bottom of the holder housed the sensor. The top and bottom part of the holder were connected with M4 screws, after placing the sensor inside the holder as shown in figure 1.2. The measuring system was thus significantly simplified compared to open measuring platform as shown in figure 1.1. The use of SMA connectors eliminated the micro-manipulators and stationary probes that greatly simplified fluid handling, but impedance mismatch was introduced.

1.5 New generation measuring platform: Closed system with metal sensor holder and co-planar waveguide

The sensor holder design was reworked and changes were made to it, using the Solidworks software. Instead of polycarbonate material, aluminum alloy was used. The new aluminum sensor holder now houses sensor as well as ceramic heating element and thermocouple underneath it.

The square shaped ceramic heater HT24S is a 20mmx20mm heating element rod compatible with Thorlabs TC200 general-purpose heater controller. This 24W (max) heating element has 50mm leads and is 1.7mm thick and can reach maximum temperature of 400°C. The temperature of the heating element is controlled using a temperature controller and a thermocouple. This allows to keep a constant temperature and also to conduct temperature studies with the help of the sensor.

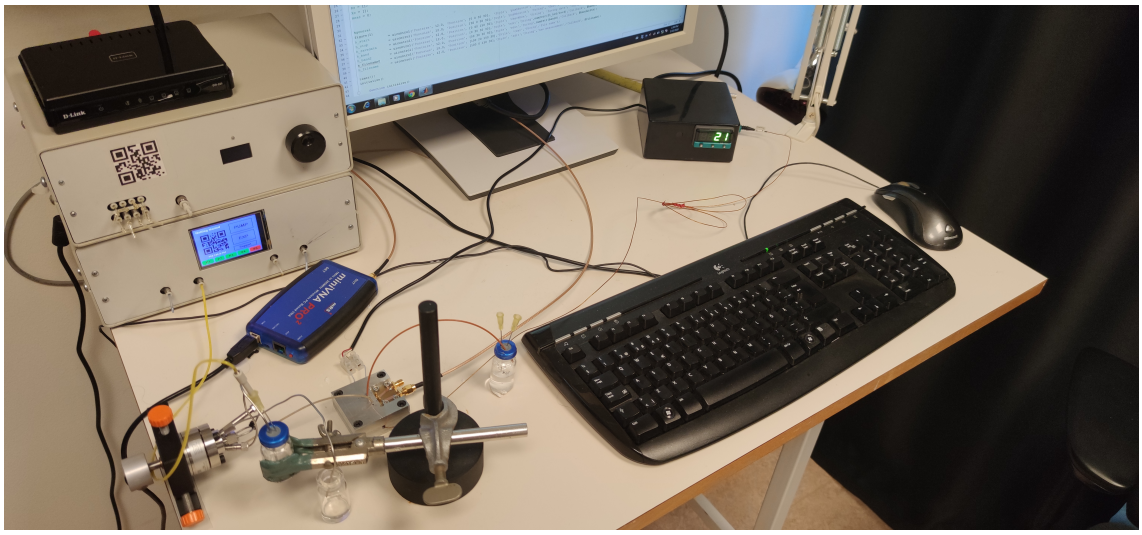

Figure 1.3: Third generation measuring platform: Closed system with metal sensor holder

The copper wire connection between chip and SMA ports were removed and a PCB with a co-planar waveguide was designed and fit into the top part of the sensor holder. The PCB was designed using Advanced Design System (ADS). Spring-loaded contacts connecting the PCB to the contact pads of the sensor, as well as SMA jacks were soldered to the PCB as shown in figure 1.3. A Mini VNA with a frequency range up to 200 MHz was replacing the stationary full range VNA.

The miniVNA PRO2 is an unique portable Vector Network Analyzer that provides a multitude of features which are intended mainly for testing antennas and RF circuits via computer. It is a wireless analyzer capable of scanning and sending the data using an integrated bluetooth module to a remote PC/smartphone within 100 meters range or via USB. It covers a range of 1MHz to 200MHz. Since the SAR sensor operates in this range, miniVNA is suitable for our measurements, despite a somewhat reduced dynamic range.

The fluid injector (a Rheodyne 6-way walve) is connected to the sensor with the help of PEEK polymer tubes. The fluid injector can be switched while injecting 40µ1 of sample fluid into the injector with the help of micro-syringes. Out of the 40µ1 of volume, 20µ enter the sensor after switching the lever to load position.

A pneumatic pressure pump is used to maintain a steady flow in the sensor. Generally, 150mbar of pressure provides steady flow in the microfluidic channels of the sensor. The flow can also be sped up to a certain extent by increasing the pressure to 250mbar. The pneumatic pump automatically adjusts the pressure in case of any interruption so as to maintain steady pressure.

MATLAB is used to generate a program that constantly records changes in the sensor. It is used to do fast and accurate real-time measurements using the sensor.

A small vial of milliQ water is connected to the flow system. During occasions when samples are not injected into the sensor through fluid injector, milliQ water in the vial maintains constant flow into the sensor in order to prevent formation of air bubbles in the channels. Small vials are also used to collect waste water at the outlets as well.

A sensor frame is also fabricated out of aluminum to house the sensor on top of the square ceramic heating element. Thermocouple is used in the sensor holder and runs beneath the sensor. It is connected to temperature controller to measure the temperature of the sensor and inturn help in maintaining the desired temperature of the sensor.

2

Theory

2.1 Sensors

All living organisms have natural sensors which will help in interacting with nature as well as protect themselves. Human beings tend to mimic nature to understand various phenomena in a scientific manner and sensor is one among them. Common examples are: the nose is a sensor to detect smell, the ears to detect sound, the eyes to detect light, etc. In places and conditions where we cannot rely on our natural sensors for accurate measurements, we use artificial/man-made sensors.

We manufacture and fabricate sensors for various applications. In our daily lives, we are surrounded by sensors. Many electronic equipment have multiple sensors. Accelerometers, gyroscopes, ambient sensors, proximity sensors, optical sensors etc. are examples.

Sensor: A device which provides a usable output in response to a specific measurand. Here, output is an electrical quantity and measurand is a physical quantity, property, phenomena or condition which is measured [1].

Transducer: A converter of any one type of energy into another [2]. All transducers are not sensors but most sensors are transducers.

Actuator: An actuator is a functional element can be used to control the flow of energy, mass or volume [3].

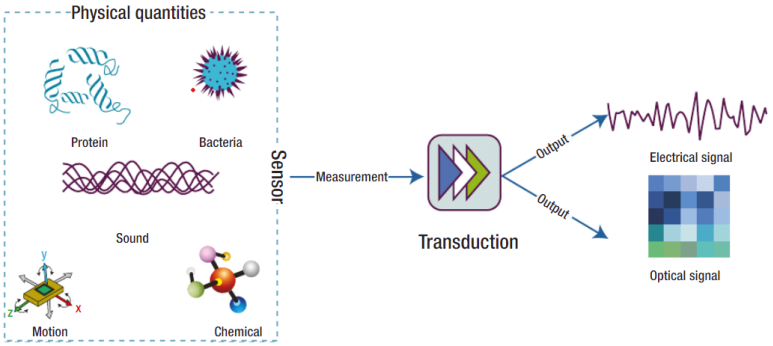

Figure 2.1: Sensing Process[1]

2.1.1 Classification of sensors [29]

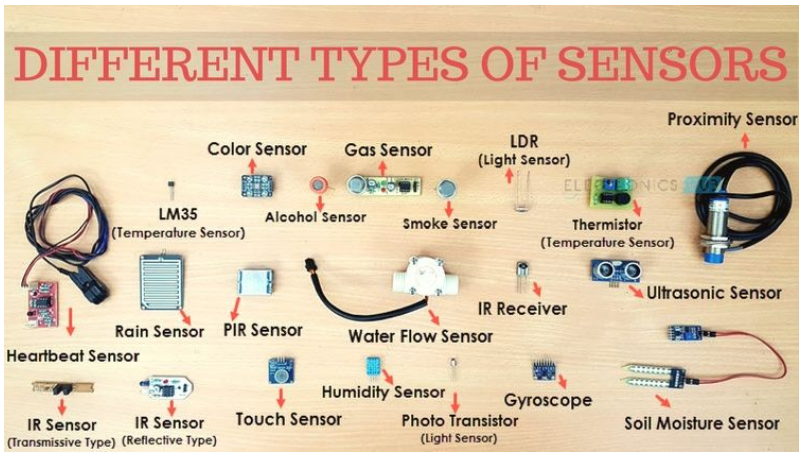

Figure 2.2: Types of Sensors (Image from https://www.electronicshub.org/different-types-sensors)

Sensors are classified into different categories based on a number of parameters. The innovation in this field is limitless and hence there is always a possibility to classify them into newer categories whenever new sensors are designed. Figure 2.2 shows different types of sensors. Few of the classifications are as follows.

- Based on the method of detection

  1. Direct sensor - Converts non-electrical parameter into an electrical signal directly, e.g. Thermocouple

  2. Indirect sensor - Transform the measurand into an electrical signal which involves a series of conversion steps with electrical signal as final output, e.g. fiber-optic displacement sensor

- Based on convenient physical parameters

  1. Active sensor - Functions with the aid of an external power supply, e.g. resistance sensors

  2. Passive sensor - Generates its own electric signal and does not require external power supply, e.g. piezoelectric Sensors, photodiode.

  3. Contact sensor - Requires physical contact with measurand, e.g. strain gauges.

  4. Non-contact sensor - These sensors do not require any physical contact with measurand, e.g. optical sensors and magnetic sensors.

- Based on the large detection area - electric sensors, magnetic, electromagnetic, acoustic, chemical, biological sensors, etc.

- Based on the physical law that govern sensors - photoelectric, photoconductive,

electrochemical sensor, etc.

- Based on the property of sensor - accuracy, sensitivity, response time, hysteresis, frequency response, resolution, linearity, cost, size, etc.

- Based on the application - agriculture, automotive, civil engineering and construction, domestic appliances, metrology, security, energy, space, military, etc.

2.1.2 Figures of merit of a sensor [30][31]

- Sensitivity is the ratio of the variation in output signal and the variation of the measured variable [4]. Sensors with high sensitivity show larger fluctuations in output as a result of fluctuations in input.

- Bandwidth or frequency response of a sensor shows how it responding over a range of different frequencies. Sensors with higher bandwidth can provide useful data for a larger range of frequencies and are able to respond to varying input.

- Accuracy of a sensor shows how close the output value of a sensor is compared to the expected/theoretical value. Sensors with higher accuracy are generally preferred because they tend to make lower errors below the acceptable level during measurements.

- Limit of detection is the smallest value of the interested parameter that a sensor can detect.

- Noise is the unwanted interference from the external surroundings including the measuring equipment that is detected by the sensor. Highly sensitive sensors are capable of detecting smallest of the noise from the external environment.

- Response time is the time required by the sensor to observe or detect the change in output as a result of change in input. Sensors with faster response time are usually preferred to detect small and rapid changes.

- Linearity is the relationship between the output values of the sensor to the input signals. Sensors are said to be linear in nature if the change in the output values of the sensors is approximately equal to the input changes detected by the sensor.

- Selectivity is the ability of the sensor to detect groups of analytes that we are interested among multiple analytes present in the surroundings. Analytes can be an element, compound, or strain of bacteria/virus that is important to the study. Good sensors are selectively sensitive in nature. Selectivity plays an important role in chemical sensor, biosensors and bio-chemical sensors.

- Repeatability is the ability of the sensor to provide the same accurate result multiple times. Sensor with higher repeatabilitiy can be used multiple times and the life of such sensors are high.

- Hysteresis is a memory effect within the system, where the response/physical quality is dependent on the previous history (of the system).

2.2 Microfluidics [5]

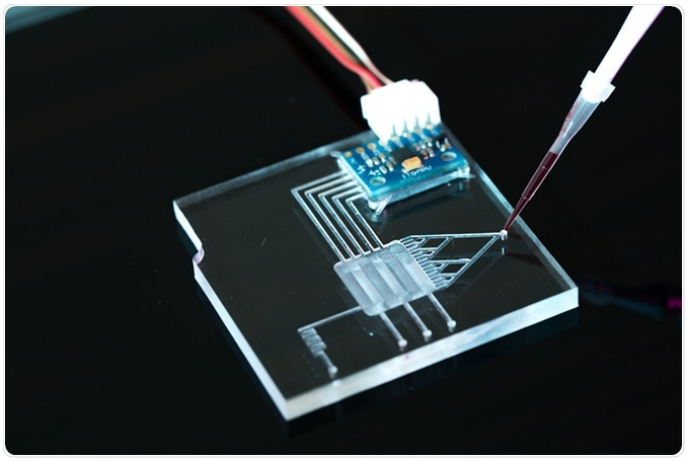

Figure 2.3: Microfluidic Chip (Image from https://www.news-medical.net/life-sciences/Protein-Interaction-Studies-Using-Microfluidics.aspx)

Microfluidics is the science and engineering of systems in which fluid behavior differs from the conventional flow theory primarily due to small length scale of the system (in the range of micrometers) and it involves manipulation of small amounts of fluids (10^{-9}-10^{-18}) in channels having diameters ranging from tens to hundreds of micrometers [6].

Fluids behave differently on this scale compared to the fluid flow at macroscale. One such phenomena is that fluids exhibit laminar flow in micro-channels which is a characteristic that is not seen in fluids on the macroscale [7]. The main advantage of microfluidics is utilizing scaling laws and continuum breakdown for new effects and better performance. These advantages are drawn out by the fact that the amount of fluids that the device can handle is less than few microliters.

Regardless of the size of the instrumentation and the type of material used in the fabrication of the microfluidic device, only the space where the fluids are processed inside the device have to be miniaturized. The combination of microfluidic systems with other technologies and the advantages of miniaturization opens up possibilities of newer horizons to explore for portable and field-deployable applications such as point-of-care testing and diagnostics.

The miniaturization and functionality of an entire lab and microfluidics led to the development of lab-on-a-chip having field-deployable applications in health moni-

toring, environmental monitoring, bio-chemical sensing, on-site nuclear testing, etc [8]. The results from this system are fast, accurate, cheap, require lower input and lower waste generation [9][10].

2.2.1 Scaling Laws

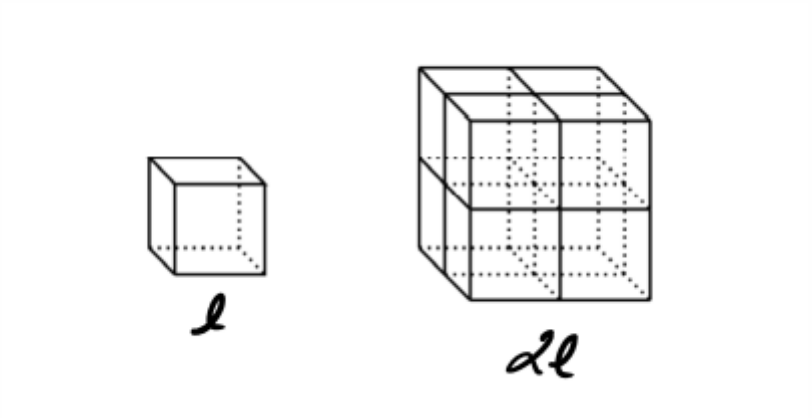

Figure 2.4: The geometric scaling of a cube. The side length of the larger cube is 2l, twice as long as the side length of the smaller cube l. Hence, the larger cube has a bottom area which is four times as large as the bottom area of the smaller cube, and the larger volume is eight times larger than that of the smaller cube.

A scaling law expresses the variation of physical quantities with the size l of the given system or object, while keeping other quantities such as time, pressure, temperature, etc. constant [32]. If scaling laws are applied to the geometry of an object in figure 2.4, any change in the characteristic length of this object will affect discrete properties differently. Similarly in macroscale, volumetric forces will be more affected by change in characteristic length than surface forces [11] since they strongly depend on the characteristic length.

$$\frac{surface\ forces}{volume\ forces} \propto \frac{l^2}{l^3} = l^{-1} \underset{l \to 0}{\rightarrow} \infty$$

Figure 2.5: Scaling law based on the characteristic length

Figure 2.5 implies that when scaling down to microscale, the volumetric forces become less important and instead the surface forces become dominant.

2.2.2 Fluid flow at microscale

The fluid flow at microscale is governed by a set of equations which illustrates the fluids' motion, pressure, and how mass transport occurs within the micro-channels. Along with the set of equations, various terms are explained which play important role in microfluidics.

2.2.2.1 Navier-Stokes Equation [33]

The motion of fluids in macroscale as well as in microfluidic systems can generally be descried by Navier-Stokes equation which is derived from Newton's second law.

$$\rho\underbrace{\left(\frac{\partial \mathbf{v}}{\partial t} + \mathbf{v}\cdot\nabla\mathbf{v}\right)}_{I} = \underbrace{\rho\mathbf{g}}_{II} \underbrace{-\nabla\mathbf{P}}_{III} \underbrace{+\mu\nabla^2\mathbf{v}}_{IV}$$

Figure 2.6: Navier-Stokes Equation

Navier-Stokes equation is describing incompressible flow of fluid of a constant viscosity. The equation is broken down and can be understood in detail. Part I gives is the change in momentum over time. It represents inertia. Part II provides information on gravitational force acting on the volume element. Part III outlines the pressure acting on the volume element. Part IV details the viscous forces.

2.2.2.2 Reynolds Number [33]

$$\underbrace{\frac{\rho v \ell}{\mu}}_{Re}\left(\frac{\partial \tilde{\mathbf{v}}}{\partial \tilde{t}} + \tilde{\mathbf{v}}\cdot\tilde{\nabla}\tilde{\mathbf{v}}\right) = -\nabla\tilde{P} + \tilde{\nabla}^2\tilde{\mathbf{v}}$$

Figure 2.7: Navier-Stokes Equation with one scaling parameter

Equation 2.1 is obtained from rearranging and simplifying Navier-Stokes equation. This simplified form Navier-Stokes equation from figure 2.7 shows only one scaling parameter which is termed as Reynolds number.

$$Re = \frac{\rho\ u\ l}{\eta} = \frac{inertial\ forces}{viscous\ forces} \tag{2.1}$$

The Reynolds number (Re) of a fluid is a dimensionless number that describes the how the fluid flow occurs across the microfluidic channels. It is the ratio of inertial forces to viscous forces that consequently quantifies the relative importance of these two types of forces for given flow conditions.

Based on the calculations using equation (2.1), at the microscale the fluids exhibit laminar flow when Re<2300 due to the dominant presence of the viscous forces and pressure. One consequence of laminar flow is that two or more streams of fluid, flowing in contact with each other will mix by means of diffusion over the length of a single channel. As the value of Re reaches a critical value, fluids tend

to start exhibiting chaotic or turbulent features and this is referred to as transient/transitional flow which exists when Reynolds number are between 2300 and 4000 (2300<Re<4000). When the value of Re is beyond 4000 (Re>4000), turbulent flow is observed due to the significance of inertial forces. It is important to note that the value of a Reynolds number is only meaningful in relation to the length scale. In microfluidic systems, Reynolds numbers Re<1 are typically observed.

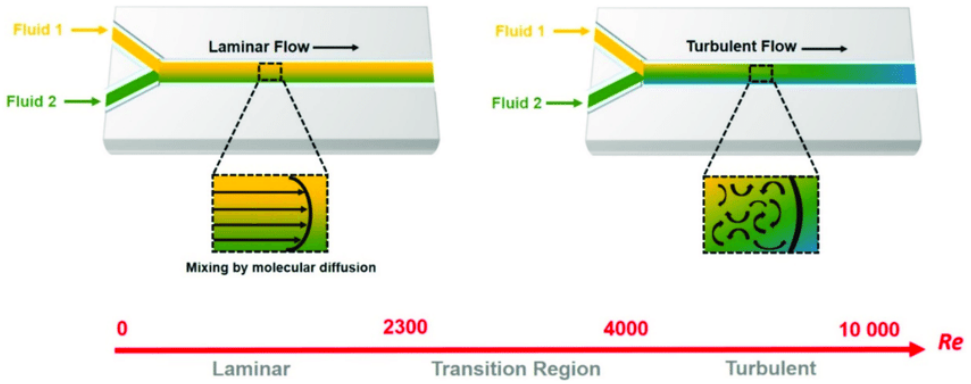

Figure 2.8: Fluid flow at various Reynolds number[35]

2.2.2.3 Mass transport at microscale

The dynamics of fluid flow at the microscale requires considering concepts beyond the Navier-Stokes equation. Mass transport in fluid flow is caused by a combination of two different phenomena: convection and diffusion.

2.2.2.4 Diffusion

Diffusion is one of the transport modes and is a random motion of particles along a concentration gradient, which results in a net flux of material from the regions of high concentration to the regions of low concentration. This type of motion is termed Brownian motion. Brownian motion continues to exist till the average concentration of particles becomes constant throughout the volume.

Diffusion is modeled in one dimension by the equation $d^2 = 2Dt$, where d is the distance a particle moves in a time t and D is the diffusion coefficient of the particle [12]. As the distance varies to the power square, it becomes very influential on the microscale.

2.2.2.5 Convection [32]

Other than diffusion, convection is transport as a result of the movement of the fluid. For pure diffusion to be considered, the velocity field of the fluid should be zero. The motion of the molecules is partly affected by convection when the velocity field of the fluid is non-zero.

The change in concentration over time in such a type of microfluidic system can be illustrated by using convection-diffusion equation.

$$\underbrace{\frac{\partial c}{\partial t}}_{I} = \underbrace{D\nabla^2 c}_{II} - \underbrace{\mathbf{v} \cdot \nabla c}_{III},$$

Figure 2.9: Convection-Diffusion Equation

The equation in figure 2.9 describes the mass transport on a microscale. Part I gives the change in concentration over time in the microfluidic system. Part II is the diffusive transport term providing information on how diffusion affects the transport in the microfluidic system. Part III is the convective transport term outlining how convection affects the transport in the microfluidic system.

2.2.2.6 Peclet Number [32]

$$St\frac{\partial \tilde{c}}{\partial \tilde{t}} = \frac{1}{Pe}\tilde{\nabla}^2\tilde{c} - \tilde{\mathbf{v}} \cdot \tilde{\nabla}\tilde{c}$$

Figure 2.10: Convection-Diffusion Equation with two scaling parameters

The convection-diffusion equation from figure 2.10 can be converted to a dimensionless form which yields two scaling parameters similar to the Reynolds number: the Pe (Peclet number) and the St (Strouhal number). The convection-diffusion equation with two scaling parameters are shown in figure 2.11.

$$Pe = \frac{\nu\ l}{D} = \frac{Convective\ transport}{Diffusive\ transport} \tag{2.2}$$

The Peclet number Pe is a dimensionless number (equation 2.2) that is a direct analogue to the Reynolds number representing the ratio of mass transport due to convection to the mass transport due to diffusion. It is useful in comparing the performance of microfluidic systems.

2.2.2.7 Strouhal number

Strouhal number is a dimensionless number that measure of unsteadiness in the flow. The Strouhal Number is necessary when analyzing unsteady, oscillating flow problems. It represents a measure of the ratio of inertial forces due to the unsteadiness of the flow or local acceleration to the inertial forces due to changes in velocity from one point to another in the flow field. It is not significant in microfluidic systems.

2.2.3 Effect of temperature in microfluidics

Temperature has an important effect on the fluids flowing in the microfluidic channels. As the temperature increases, the viscosity of the fluids decrease which leads to a faster fluidic motion through the channels of the microfluidic device. A rise in temperature in the microfluidic environment heats up the fluid in a rapid manner since the amount of fluid flowing through a cross-section of the channel is in the order of microliters.

2.2.4 Advantages of Microfluidics

- The amount of sample used in microfluidic system is very low.
- Improved analysis and faster detection speeds
- Compactness
- Cost reduction
- A range of micro-domain effects is present
- Portability
- Ease of use and Ease of fabrication
- Multiple analytes can be processed simultaneously in small devices, providing access to high-throughput applications.
- Reduced processing time and increased productivity, allowing for ease of integration into a variety of experimental systems.

2.2.5 Applications of Microfluidics

Microfluidics has a wide range of applications, with a notable example in ink-jet printing. Modern applications are in the field of life sciences and analytical chemistry are increasing steadily in numbers. The field of biology has been using microfluidics for studying cells as the dimensions of the cells and the microfluidic channels are similar. Their applications extend to analytical purposes such as diagnostics, sensing, or sample processing.

Point-of-care applications are becoming possible due to the portable nature of microfluidic systems. Complex experimental setups are being successfully reduced to microscale systems. Due to their small size and faster, accurate processing, they are cost-effective and can be single-use, avoiding cross-contamination. Lab-on-a-chip, cell-on-a-chip and organ-on-a-chip are such complex systems that are being used in analytical and pharmaceutical research and work.

More and more applications are emerging continuously. Microfluidics are being integrated with existing systems and hence can provide new purpose to existing

technologies as well. One such example being Surface Acoustic Wave sensors.

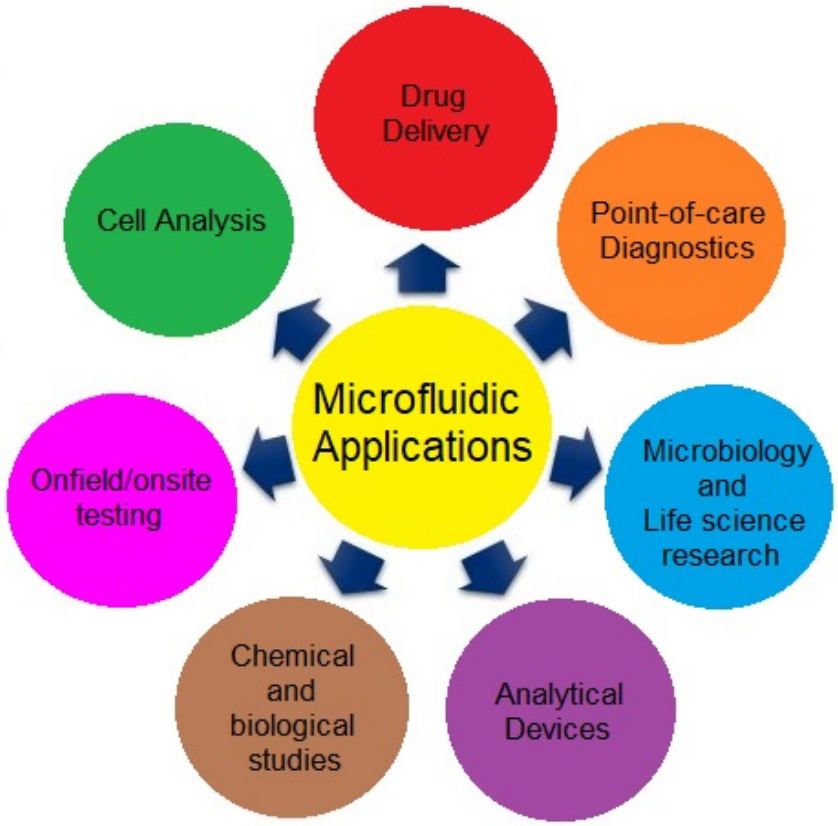

Figure 2.11: Overview over application areas of microfluidics

2.3 Acoustic Waves in Solids

Acoustic waves are mechanical waves that propagate in elastic solids by means of adiabatic compression and decompression [13]. First described by Lord Rayleigh in 1885, acoustic waves exhibit common wave phenomena like diffraction, reflection and interference [13]. Unlike bulk acoustic wave (BAW), surface acoustic waves (SAW) are confined near the surface. This confinement of energy in SAW devices has found applications in various fields. SAW belongs to the family of guided acoustic modes [13].

2.3.1 Classification of acoustic waves

Acoustic waves are classified into three groups [34]:

- Bulk Acoustic Waves: They are elastic waves which propagate through the solids. Based on the direction of propagation of BAW, they are classified into longitudinal waves (L-type or pressure waves) and shear waves (S-type waves) .

  L-type waves travel in parallel to the direction of propagation in the solids

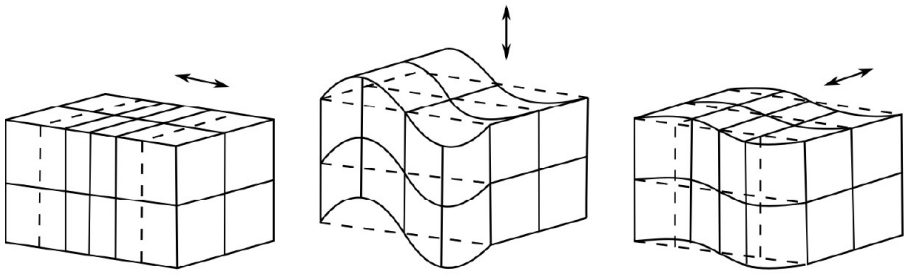

(a) *Longitudal bulk acoustic wave* (b) *Shear vertical bulk acoustic wave* (c) *Shear horizontal bulk acoustic wave*

Figure 2.12: Classification of Bulk Acoustic Waves (BAW)

whereas S-type waves travel perpendicular to the direction of propagation in solids .

Shear waves are two components based on the specified propagation direction: Wave with shear-vertical polarization (SV-type) and wave with shear-horizontal polarization (SH-type) .

BAW suffer attenuation of their amplitude while propagating in the solids due to losses scattering of the wave propagating through inhomogeneous media and through thermal lattice vibrations. Only L-type waves exhibit another type of loss of amplitude due to temperature variation within the solid [14].

- Acoustic Plate Modes: They are classified into two categories - Lamb Waves and Shear plate modes. Lamb waves are elastic waves whose particle motion lies in the plane containing both the direction of wave propagation and the plane normal. Lamb waves are wave with polarization in sagittal plane. Shear plate modes are SH-type waves that propagate in plates [19].

- Surface-guided Acoustic Waves: They are only found on surfaces of solids or on the interfaces of solids and other matter. The Rayleigh acoustic wave, Love wave, Leaky surface wave and Bleustein Gulyaev wave are the 4 categories of surface waves that are classified as surface-guided acoustic waves .

  Rayleigh acoustic waves (RSAW) is a surface-guided eigenmode which is formed due to the coupling of L-type wave component and SV-type wave component present close to the surface . The reason behind coupling is due to the fact that unlike SH-type waves, L-type and SV-type wave components alone are not fulfilling the zero normal stress boundary condition at the surface and thus can't freely propagate in parallel to the surface [15].

  Some materials possess a very specific crystallographic symmetry due to which they have a pure SH-type SAW propagation mode, specifically the Bleustein Gulyaev (BG) wave [16].

  SH-type SAW's can also appear in layered materials with low shear wave

velocity. These waves are referred to as Love waves [17].

When SH-type wave no longer concentrates its energy close to the surface, these waves still propagate while accompanied by a weak-amplitude slow shear bulk wave radiation into the substrate. This leakage will result in attenuation of the wave. These type of waves are called Leaky surface acoustic wave [18].

Important features that define the properties of surface acoustic waves on piezoelectric substrates are [14] [34]:

- SAW velocity: A constant relating the frequency ω and magnitude of the wave-vector k .
- Piezoelectric coupling constant/electromechanical coupling constant (K^2): A numerical measure of conversion efficiency between electrical and acoustic energy in a piezoelectric material . In SAWs, K^2 is defined in the same way as for the BAW. It is the relative velocity shift of SAWs propagating under electrically free and metallic surfaces respectively .

$$K^2 = \frac{2(V_f - V_m)}{V_f} \tag{2.3}$$

  where, V_f and V_m are SAW velocities on free and metallized surfaces of a piezoelectric material
- Temperature Stability: It is important for continuous performance within the defined specification over a course of time.
- Beam Steering: It occurs when the direction and the speed of the power flow do not coincide with the direction and speed of the wave vector. The propagation speed of power flow or group velocity defines a technological requirement of how precisely piezoelectric crystals have to be grown and cut, along with how accurately the elements that excite acoustic waves have to be aligned with orientation of a substrate .
- Material-related losses: It is due to thermal lattice vibrations, surface roughness, leakage into air, etc. Generally shear waves possess lower propagation loss when compared to the longitudinally polarized waves and materials with larger electromechanical coupling tend to show higher propagation losses .
- Permittivity: It determines the capacitive impedence of the excitation metallization that is often designed to be around 50Ω in order to get a perfect matching with the peripheral electronics .
- Propagation losses: SAW energy can often scatter into bulk modes through diffraction or surface perturbations. It is also possible for bulk modules to be genrated directly at the surface. These effects lead to spurious responses that have to be suppressed in practical device design .

- Quality Factor: It is the ratio of the stored energy and dissipated energy for one wave cycle. It is one of the most important parameters characterizing resonator performance. It is a measure of relative loss of energy (acoustic, electric and dielectric losses) in a resonator .

$$Q = \omega \frac{Energy\ Stored}{Power\ dissipated\ per\ one\ cycle} \tag{2.4}$$

2.4 Microelectromechanical systems (MEMS)

MEMS is a technology that integrate mechanical and electrical components into micro-devices. The dimensions of MEMS vary from few millimeters to micrometers in size. These devices have the ability to sense, control and actuate on the micro scale and generate effects on the macro scale [24].

The interdisciplinary nature of MEMS utilizes design, engineering and manufacturing expertise from a wide and diverse range of technical areas including integrated circuit fabrication technology, mechanical engineering, materials science, electrical engineering, chemistry and chemical engineering, as well as fluid engineering, optical technology, cleanroom technology instrumentation and packaging [24]. MEMS technology has found numerous applications in all fields ranging from microgears in watches to system-on-chips (SOCs) processors in our laptops, mobiles and other daily-driver electronic devices. Some of the current generation applications of MEMS technology include accelerometers for airbag sensors, inkjet printer heads, computer disk drive read-write heads, projection display chips, blood pressure sensors, optical switches, microvalves, micropumps, biosensors and many other products are commercially manufactured in high volumes [24].

Even though MEMS technology is complex and expensive, the accuracy, life-span and efficiency of the devices is unmatched by other technologies. Another advantage is that MEMS can be manufactured with the existing and familiar cleanroom fabrication techniques. The ability to easily integrate newer technologies with MEMS will drastically reduce the space occupied by the otherwise large equipment and make the devices more compact. Piezoelectric sensors are an important class of analytical sensors which utilises MEMS technology in architecture as well as in the fabrication process.

Piezoelectric sensors are a class of analytical sensors which utilises MEMS technology in architecture as well as in fabrication process.

2.4.1 Piezoelectric materials

Piezoelectric materials are a class of materials which have found applications in a variety of technological fields, due to their special properties: when subjected to a mechanical stress, the electric polarization in these materials change, whereas when an electrical charge is applied on the material, it experiences mechanical strain in the form of acoustic waves. Acoustic waves and their classes are explained in an earlier context. Some naturally occurring piezoelectric materials are quartz, topaz, etc. These materials have lower degrees of piezoelectricity than synthetic/man-made piezoelectric crystals such as aluminium nitride, lithium niobate, lithium tantalate etc. Piezoelectric materials have been used in RF filters for a long time. An important group of piezoelectric devices that generate surface acoustic waves are surface acoustic wave sensors.

2.4.2 Surface Acoustic Wave (SAW) Sensors

Surface acoustic wave sensors are a class of microelectromechanical systems (MEMS) which rely on the modulation of surface acoustic waves to sense a physical phenomenon. The sensor converts the input electrical signal into acoustic waves which can be easily influenced by physical phenomena. The device then transduces this wave back into an electrical signal. Changes in amplitude, phase, frequency, or time-delay between the input and output electrical signals can be used to measure the desired phenomenon.

2.4.2.1 Layout of a SAW sensor [14]

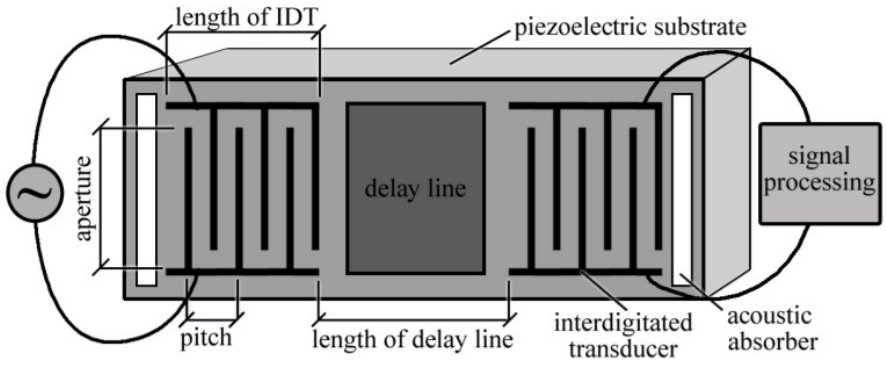

Figure 2.13: SAW sensor (Image from http://www.jaredkirschner.com/)

The basic layout of a SAW device consists of a piezoelectric substrate with an input interdigital transducer (IDT) on one side of the substrate and an output IDT on the other side of the substrate. The region between the IDTs across which the surface acoustic wave propagates is called the delay line. The region is termed as delay line due to the fact that the signal produced by the input IDT is a mechanical wave which moves much slower than its associated electromagnetic form, causing a measurable delay in this region.

Interdigital electrodes (IDTs) consist of several comb-like structures are fabricated from thin metal films on top of the substrate using the existing semiconductor industry processes. The IDTs can be designed to generate SAWs in specific patterns for different applications.

As a result of the piezoelectric effect, when electric voltage of a certain frequency is applied to the input IDT, the resulting electric field will cause mechanical strain on the substrate [25]. The mechanical strain will in turn cause waves to spread on the surface. The most important factors determining the IDT characteristics are the finger geometry in the period, the overall number of finger pairs, and the substrate material. In a similar way the output IDT converts the waves caused by mechanical strain into electrical signals.

The substrate used for SAW devices are materials capable of exhibiting piezoelectric effect. As all piezoelectric materials are anisotropic in nature, the material properties are not only dependent on the material itself but also on the cut angle and the SAW propagation direction. The substrate piezoelectric materials generally used for SAW devices are quartz, $LiTaO_3$ and $LiNbO_3$.

SAW sensors sometimes include an additional element to sense various types of phenomena indirectly.

2.4.2.2 SAW device configurations

Typically, SAW devices use either a one-port resonator or a two-port resonator. One-port SAW resonator uses the same port for both input signal and output signal which makes the device more compact in nature. The one-port configuration is more robust and reduced size which allows for easier integration, lower data processing, lower losses and strong resonance characteristics. The one-port configuration induces damping of SAW as the liquid required to study has to be over the surface of sensing region which includes IDT, resonators and device surface. This prevents the use of one-port SAW resonators as liquid-phase sensors.

Two-port SAW resonator was designed in order to improve upon the problems plaguing the delay line topology. In order to reduce losses to minimum, the wave propagation mode has to be carefully picked which includes choice of substrate, materials, dimensions, IDT and design. Two-port SAW resonator sends and receives electrical signals two different ports and hence the waves are constantly travelling between the two transducers which affects integration and miniaturization of the device. Figure 2.14 shows an example of a two-port SAW device.

2.5 New SAR concept

The combination of microfluidics, acoustic waves and sensing technology led to the development of microfluidics-based SAR sensors. The presence of microfluidic-SAR sensor interface creates a favorable environment for the surface acoustic waves generated by the piezoelectric substrate to interact directly with the small quantities of

fluids (in microliters) flowing in the microfluidic channels. If there are any changes in the fluidic environment (change in the fluid) of microchannels, there will be changes in the acoustic waves and these variations are monitored in real-time.

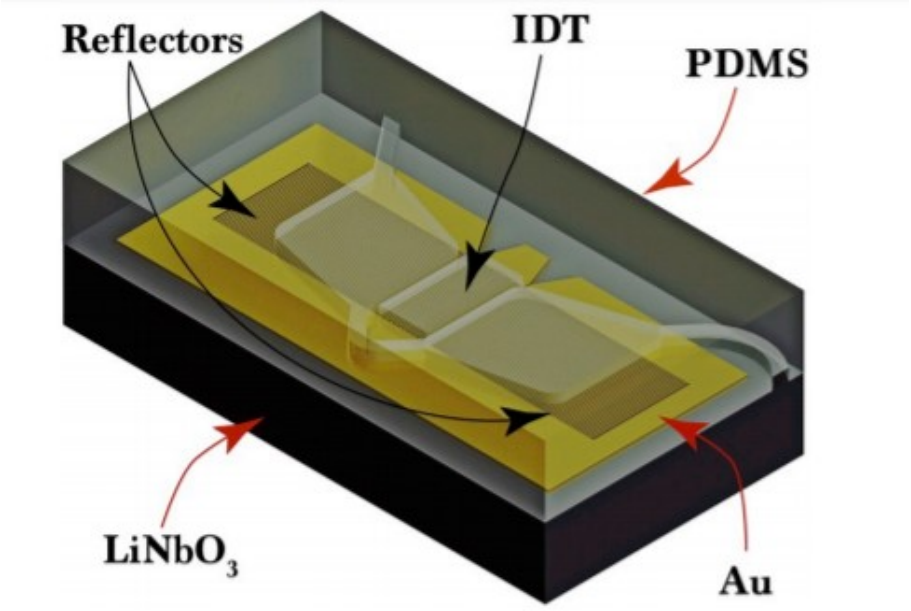

Figure 2.14: SAR sensor design [20]

SAR based liquid sensors are more sensitive than QCM sensors due to the fact that sensitivity scales with frequency. This has to be weighed against the electronic interferences, which also increase in intensity with frequency. SAR sensors generating Rayleigh waves experience strong attenuation of acoustic energy upon liquid contact during its operation [21] and hence SH-SAWs such as Love waves and leaky SAW waves are used more often for in-liquid measurements. In order to prevent large transmission losses and shot-circuiting of SAW transducers by liquid conductivity, soft polymer polydimethylsiloxane (PDMS) based microfluidic system was integrated over the sensing area of the SAW sensor for the sake of liquid confinement at the expense of additional damping losses [22].

A frequency shift is observed when measuring the mass of an adsorbed analyte using SAR sensor. The frequency shift of SAR sensor is:

$$\Delta F = -k f_0^2 h \rho \tag{2.5}$$

where, k is constant related to substrate and device properties, f_0 is resonance frequency of the device, h and ρ are thickness and density of the layer. The resonant frequency of the SAW sensor has linear motion to mass loading:

$$\frac{\Delta F}{f_0} = -k \frac{h}{\lambda} \rho \; v \tag{2.6}$$

where $\frac{\Delta F}{f_0}$ is relative frequency shift, $\frac{h}{\lambda}$ is layer thickness to wavelength ratio and v is velocity of SAW. The amplitude and phase characteristics are obtained from the dispersive reflection of SAW from metal strip gratings on both sides of the IDT.

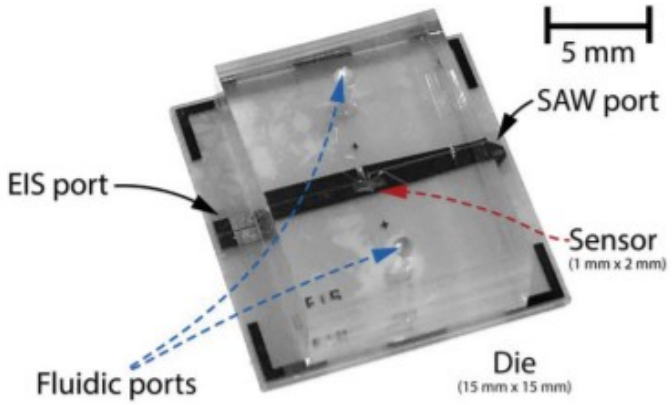

Figure 2.15: SAR sensor with microfluidic channels [26]

A newly developed lateral energy confinement reflector topology of the SAR sensor offers significantly increased sensitivities compared to any other explored SAW sensor approaches, while maintaining similar noise levels [26].

The reflective gratings of a one-port SAW resonator act as sensing elements, while the wideband IDT is protected from the liquid by positioning between the reflectors and thus providing low susceptibility to damping [25]. It also gives control over the device impedance and provides simplified measurement setup [25].

This innovative sensor design enables integration with low frequency impedance microscopy (EIS). For this implementation, Au gratings were arranged in an interdigitated manner forming a capacitor enabling simultaneous and acoustic resonance-independent electrical measurements of dielectric permittivity near the sensing surface [27].

2.5.1 Electrochemical impedance spectroscopy

Electrochemical impedance spectroscopy (EIS) is a powerful technique used to analyze electrical impedance of a system by detecting changes at its sensing surface and characterize systems by their dielectric properties. Spectroscopy is rather a term that is used as impedance of the SAW sensor is studied at different frequencies. All sensor holders of measuring systems that were developed in this project support multi-parametric sensor studies, as they have an additional EIS port for impedance measurements. EIS is typically used in analysing corrosion mechanisms, membrane transport properties, monitor cell mechanisms and also useful in conducting biosensing and analytical studies.

2.5.2 Materials used

The piezoelectric substrate material used in SAR/EIS sensor is the Y-cut X-propagating $LiNbO_3$. It is a synthetic ferroelectric crystal that possesses a very large dielectric constant and piezoelectricity (K^2) [14]. In addition to this, it also has a large py-

roelectricity and electro-optic effect [14]. K^2 for Y-cut LiNbO3 for some rotation angles can be as high as 25% and it produces a leaky SAW (LSAW) propagating along the X-axis of the substrate with the propagation velocity of leaky SAW of about 4200 m/s [14]. Thus, low impedance SAW sensors sustainable to viscous loadings can be constructed as most of electrical energy is converted to LSAW The high degree of piezoelectricity of the $LiNbO_3$ makes it very sensitive towards variations on its surface. The temperature coefficient of velocity is about -75 $ppm/°$C [9].

LSAW suffers from bulk scattering losses and thus the acoustic energy at the surface decreases leading to reduced sensitivity. This is overcome by using gold (Au) periodic strip gratings which slows down LSAW and converts it into surface-guided SH-SAW [27].

The microfluidic sample processing and delivery parts of the sensor were fabricated from PDMS. PDMS is a semi-transparent organo-silicon polymer, easy to mold into any design, easy to use with our mold system, capable at handling high pressures due to its rubbery nature, non-toxic and does not interact with majority of the fluid samples. Although not compatible with organic solvents and very hydrophobic analytes, it is a suitable candidate for many applications of microfluidic chips.

2.5.3 Effect of Temperature on SAR sensor

Temperature variations in environment and high power input operations affect the sensor temperature. The temperature coeffiecient of frequency (TCF) is used to describe sensor's frequency stability as a function of temperature. The variation in temperature causes frequency drift which is constant for a given crystal cut and technology. Temperature stabilised resonators can be developed when the TCF values are known. The practical solutions to deal with frequency drift is to use crystal cut with zero order TCF, or by amalgamation of two materials with TCF opposite in sign. Hence $LiNbO_3$ and SiO_2 were used as they have negative TCF and positive TCF respectively in the development of SAW sensors. High performance temperature compensated zero TCF resonators use novel heteroacoustic layer substrates as well.

3

Methods

This chapter describes the process of fabrication of SAR sensor and its measurement system beginning with the design of polycarbonate molds.

3.1 Design

The first step in fabrication of SAR sensor and the development of its measurement system designing and simulations. The designing of the SAR sensor, a planar multi-layer device, was performed with AUTOCAD, whereas the designing of microfluidic sample handling device for the sensor and the sensor holder required a 3D software (SOLIDWORKS). AUTOCAD was also used for the purpose of creating designs for integrating a multifunctional microfluidic pipette with the SAR sensor, and SOLIDWORKS for designing microfluidic various molds and support systems. The mold systems for the multifunctional microfluidic pipette was far more demanding compared to the mold system for the simple microfluidic sample handling chips used in the project. Similarly, a holding scaffold for the microfluidic device was designed and tested. We faced the challenge that the holding interfaces have to be as small as possible to allow for application under a microscope, but must also provide adequate mechanical support to both the sensor and the microfluidic device.

3.1.1 Design of a SAR sensor

The SAR sensor involves designing of the piezoelectric surface of the sensor and microfluidic system of the sensor. The piezoelectric surface of the sensor consisted of designing IDTs, resonator, sensing regions, etc. The structures were such that it converted LSAWs completely into SH-SAWs in order to amplify the sensitivity of the sensor as well as to confine acoustic waves to the sensing region.

The microfluidic system was designed such that 20μl of fluid could be injected at once. The presence of microfluidic system protected the sensing region from short-circuiting due to fluids flowing on it. It consisted of a pair of microfluidic containers separated by an air cavity in between so that the fluid is held in the sensing region long enough to get a frequency change while measuring. 2 microfluidic channels entering and leaving the sensing region were also present to bring the fluid samples into and out of the sensing region via two ports. These microfluidic channels were

designed to be 50μm in width. The length of these channels were several mm, such that if the sensor is heated in the scaffold, the fluid sample injected into the microchannel can assume desired temperature as it travels through the length of the channels to the sensing region.

Moreover, designing of proper alignment marks on wafers are essential for later combination of the diced wafers with the PDMS devices. Proper alignment with micrometer precision is required for the preparation of high quality sensors.

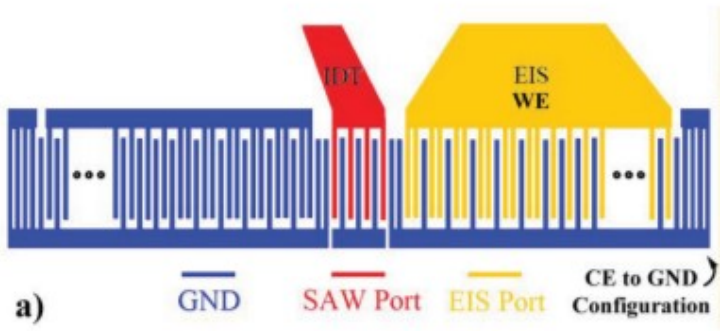

Figure 3.1: Schematic view of the SAR design (EIS section: WE -work electrode, CE - counter electrode and GND - ground) [20]

3.1.2 Design of Mold system for microfluidic chips

The microfluidic mold system was produced in order to ease the handling and curing of PDMS during the soft lithography process of fabrication of microfluidic system for SAR sensors. This concept provided more control over minute details, which prior to this, complicated the fabrication of microfluidic system. The mold system was fine-tuned in order steadily improve the fabrication process.

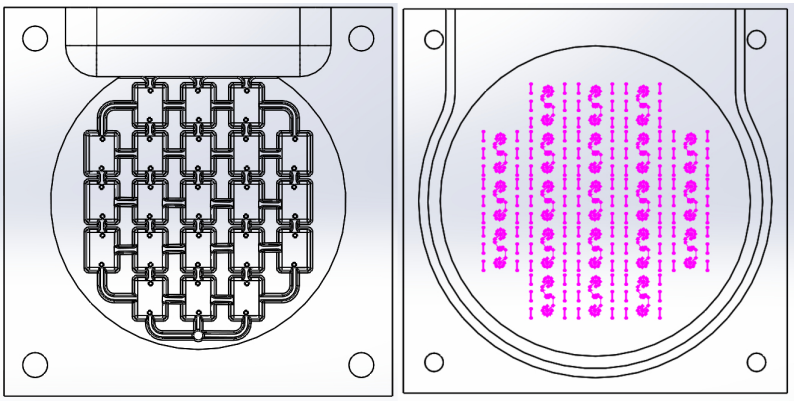

Figure 3.2: Designs of top and bottom part of microfluidic mold system

The design for the PDMS mold consisted of the SU-8 structured master wafer fabricated with microfluidic channel system, a adhesive tape to hold the master; top and bottom part of the molds which gave the required shape to the microfluidic

chips used in the fabrication processes. The bottom part of the mold was made of aluminum. The silicon master was fitted to it, and a rubber ring of diameter 3mm, surrounding the master, was introduced to prevent leaking of the initially fluid PDMS. Aluminum also gave the required rigidity to the mold. The top part of the mold was made of transparent polycarbonate, which is important for alignment of top and bottom. The mold is aligned such that microfluidic channel system on the master wafer matches its microfluidic chip counterpart, and locked with the help of the screws. The rubber rings gives a very small leeway in between the mold parts, preventing damage to the master.

The key aspects to be noted while designing microfluidic mold system are:

- Rounding the corners of structures are important in order to prevent entrapment of air bubbles. The corners and sharp edges are hotspots for bubble entrapment. Rounding corners by 0.1-0.8 mm will negligibly inflict the design, but allows for smooth flow of air bubbles.

- The mold needs channels connecting all the microfluidic chip designs so as to have a easier and free flow of PDMS while filling up the mold.

- An outlet channel is required so that the air bubbles can freely exit the mold system. The channel is to collect air bubbles generated within the mold system.

- A plate is to be screwed tightly onto the outlet channel so that PDMS does not flow out of the mold.
- A trough is required and can be of the same volume as the entire microfluidic system of the mold so as to hold the entirety of PDMS poured into the mold. It is to be at the top of the microfluidic system to facilitate downward filling of the PDMS.
- It is also important to take the volume shrinking ratio of PDMS into account as PDMS shrinks about 1% to 2% when it cures upon heating, which means that the microfluidic system design of the mold needs to be 1% to 2% larger than the desired size of the finished microfluidic chips. Hence the structures on the top part of the mold is scaled up by 1.0192 to account for the PDMS shrinkage.
- Tolerances of the structures are to be considered while designing the structures because none of the mechanical tools can give exact dimensions as we require and hence having a foresight to include tolerances with the dimensions of the structures is crucial.
- 3-D depth perception is important while designing as assigning incorrect depth to the structures produces microfluidic chips with wrong dimensions or in some cases can lead to wrecking of the master wafer which is time-consuming and expensive.
- Screw holes on the top part of mold must be a bit bigger in diameter compared to screw holes on the bottom part of the mold to facilitate alignment of microfluidic structures.
- Designing must be done to facilitate easier removal of waste cured PDMS from the mold.
- Disassembling of the mold after fabrication is to be considered and all the features such as holes for air injection, lower depth for rubber rings, etc that support easier handling of disassembly is essential.
- Holes where the parts of molds are screwed together are supposed to be nearer to the rubber rings to prevent leakage of PDMS after casting.
- Final analysis is required once the designing is done before being fabricated.
- Once fabricated, flaws in the microfluidic mold systems are to be noted down and the design for the next generation has to be rectified.

3.1.3 Design of Sensor Holder

The new sensor holder plays an active and important role in the sensor measurement system. I designed three different types of sensor holders which facilitated the

measurements. The first iteration was a polycarbonate sensor holder which was used for several measurements. The second generation of sensor holders were made of aluminum and had two designs to facilitate varying measurements.

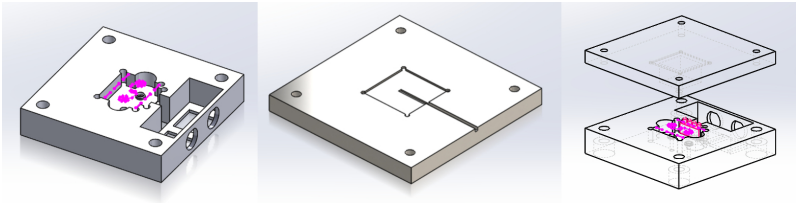

Figure 3.3: First iteration designs of top and bottom parts of sensor holder along with their assembly

The first iteration of sensor holders were for proof-of-a-concept which was thought up to overcome interference of noise from external environment. This design allowed for a smooth and successful transition from open sensor measuring system to closed system.

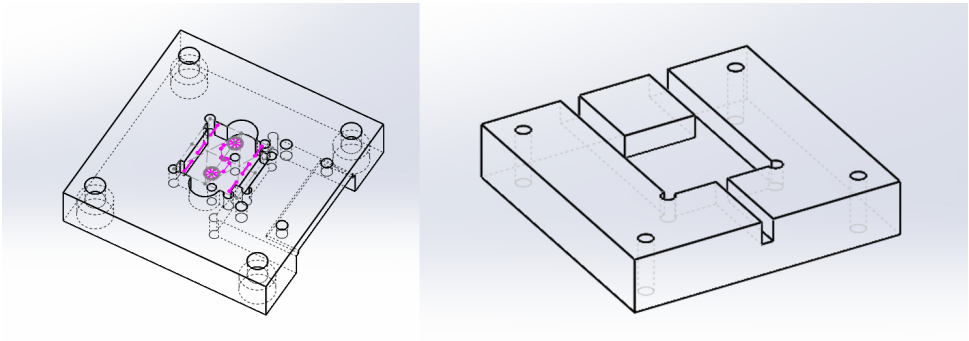

Figure 3.4: Second iteration designs of top and bottom parts of sensor holder

The second iteration of sensor holders was created to overcome disadvantages from the first iteration of holders. Thus, two different sensor holders for different measurement purposes were designed. Sensor holders became more sophisticated in function but simpler in construction, and also maintained the same footprint of the previous generation sensor holder. Special software (ADS) was used to design an interface PCBs, which was integrated into the sensor holder, such that the use of wires was completely eliminated. The PCB design consists of a co-planar waveguide which matches the impedance of the connector to the sensor chip and reduces signal loss in the interface.

The key design aspects to be noted for the holders are similar to that of designing the microfluidic mold system, but both electrical and fluidics parameters have to be considered in this regard:

- The sensor slot in the holder should be a tiny bit larger than the sensor size. The thickness of the slot also should be a bit more or equal to the thickness of the SAR sensor.

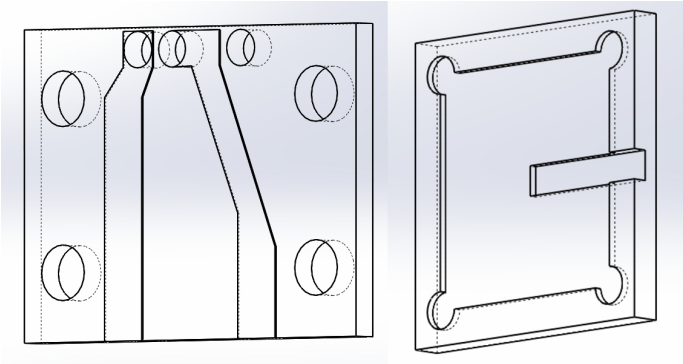

Figure 3.5: PCB design and sensor frame designs of second iteration sensor holders

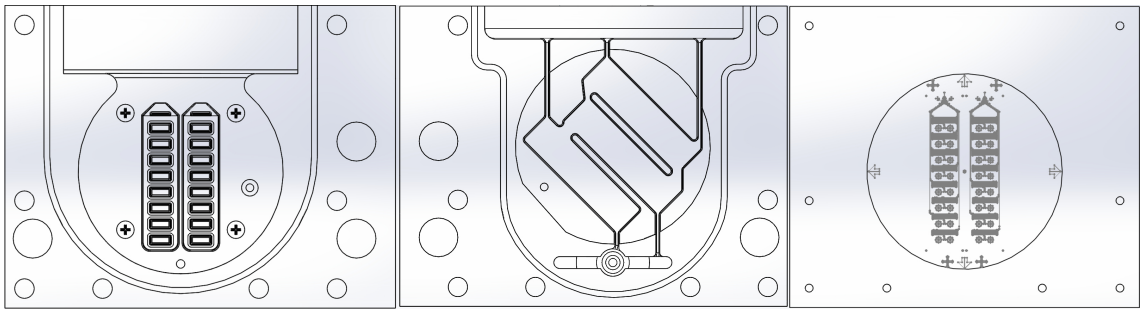

Figure 3.6: Big multifunctional pipette mold system: front design, back design and back plate design with master

- The sensor slot should have circular indentations at all the 4 corners which would help while CNC machining the sensor holder.
- All electrical connectors have to be soldered into the PCB and then connected to the sensor holder.
- The thermocouple slot which holds thermocouple should extend underneath to the center of the sensor for accurate temperature measurement.

3.1.4 Design of a mold system for the multifunctional microfluidic pipette

Multifunctional microfluidic pipette is a microfluidic open volume device for sampling of analytes from open containers, culture plates, petri dishes, etc. It is created and optimized to fit into practically any micro-manipulation environment. The large multifunctional pipette, based upon a previous, smaller design, is an open volume microfluidic system designed in order to incorporate the SAR sensor with its microfluidic system.

The mold system consists of flow channels for PDMS on both sides of the mold. This design was created in order to introduce PDMS by pouring rather than injecting, which simplifies the process, and ensures that the minimal amount of PDMS is utilized. For that purpose, a U-flow system was invented. PDMS is poured into the

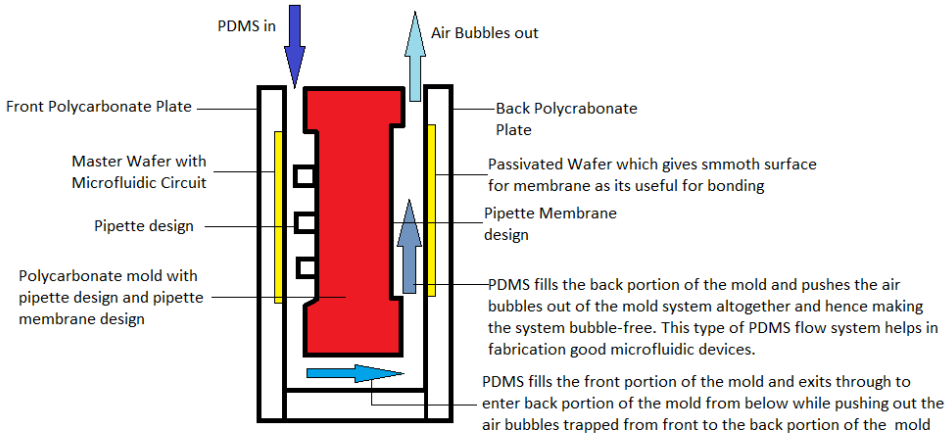

Figure 3.7: U-Flow system designed for PDMS flow in multifunctional pipete mold system

front portion of the mold, the PDMS slowly occupies all the regions in the front part and the excess PDMS would enter the back portion of the mold through a port from beneath the pipette structures of the front mold. Now PDMS can rise through the back portion of the mold and pushes air bubbles out of the mold system from the back. The U-flow system is explained schematically in figure 3.7. It is to be noted that the microfluidic mold systems for the large multifunctional pipettes is similar to an earlier developed system. The new mold, based upon a 4" wafer, can fabricate two large devices and associated structures at a time due to its larger dimensions, whereas the previous mold was designed for four small devices and support structures at a time.

3.1.5 Design of the big and small multifunctional pipette holders

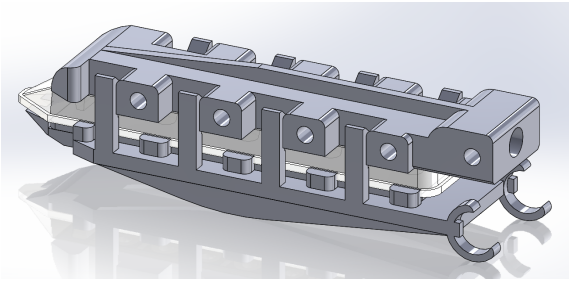

Figure 3.8: Assembled small multifunctional pipette holder with small pipette in between (highlighted)

When multifunctional microfluidic pipettes are used, there has to be continuous pressure applied on the wells of the pipettes to control fluid flow inside the microfluidic channels. Hence 8 pressure tubes are to be attached onto the wells through a designated pipette holder. The finger-like structures on the bottom part of the holder help in quick locking and unlocking with the top portion of the holder. They

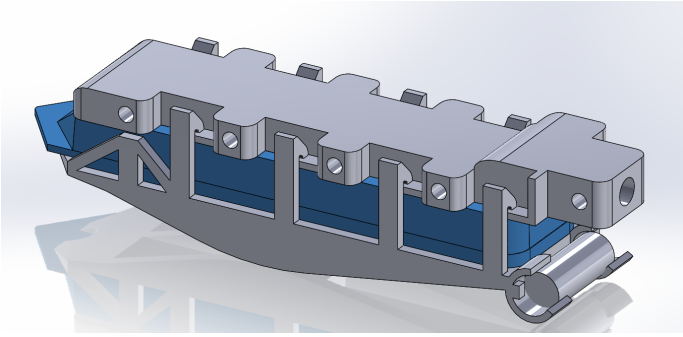

Figure 3.9: Assembled big multifunctional pipette holder with big pipette in between (highlighted)

also help in creating vacuum seals across the wells, which is of critical importance. Since the holders are small in width but long in length, they tend to bend after fabrication due to which the vacuum seal in the front portion of the wells is lost, the finger-like structures and the fin-like structure on the top and bottom holders are here to prevent the bending and preserve the vacuum seals. when assembled, the devices and top holders can slide into small slots, where it locks with the finger-like structures.

3.2 CNC Simulation

The designs of sensor holders, mold system for microfluidic chips and mold systems for the big and small multifunctional pipettes are exported as .stl files onto a simulation and CNC process generation software MayKa. It is used to generate a 3D simulation model and execute all the processes created for CNC machine to cut the required structure out of a block of polycarbonate/aluminum block. The simulated model ensures whether the processes generated are successful in obtaining the desired product or if otherwise the tools or the processes have to be tweaked and changed to our liking.

Once the .stl files are uploaded, the origin is fixed and the surface to be cut on CNC is selected. Next, a cutting method is selected. The types of cutting methods that can be simulated in MayKa are: sweeping, Z-cutting, horizontal cutting, non-horizontal cutting, contouring, plunge-cutting and surfacing. For majority of the structures that are to be cut, only sweeping and Z-cutting processes are sufficient. Sweeping, as the term states, sweeps in X and Y axes across the region selected on the surface to be cut. Z-cutting cuts entire selected region along the z-axis before moving on to the next specified region of the surface. Based on the requirement the process type is selected, the type and dimensions of the tool is selected and mentioned. Then roughing/finishing is selected and the depth cut pass and increment is mentioned. Finally spindle speeds and feed rates are entered based on the type of material block selected. The simulated 3D analysis is generated. If the simulated results are satisfactory, the process is exported to CNC machining software GPilote.

3.3 CNC Machining

A CNC machine is a computer controlled machining tool with a motorized maneuverable platform. Instructions are delivered to a CNC machine in the form of a sequential program of machine control instructions and then executed to obtain desired structures. The program can be written by a person or generated by graphical computer-aided design (CAD) software. A CNC machine processes a piece of material (metal, plastic, wood, ceramic, or composite) to meet the specifications by following a coded programmed instruction or graphical computer-aided design (CAD) which are created and input by a person.

3.3.1 CNC Machining of mold system for microfluidic chips

It is to be noted that cutting a polycarbonate block requires high spindle speeds of 21000 rpm and higher feed rate of 20mm/s as lower spindle speeds and feed rates lead to melting of plastics and result in the tools getting stuck in the material. There are single tooth cutters with polished flute of several diameters (6mm, 3mm, 2mm, 1.5mm and 1mm) of varying lengths used for cutting the polycarbonate block.

An important aspect to be remembered is that cutting an aluminum block requires lower spindle speeds of around 10000-15000 rpm and lower feed rate of 3-5mm/s as higher speeds rapidly reduces durability of the tools and the chances of breaking a tool is high. The metal cutting is mostly done with oil as lubricant continuously flowing on the metal surface to prevent it from heating. The tools used in this case with the presence of oil are double tooth cutter with or without Titanium Aluminum Nitride (TiAlN) coating. Since this type of metal process is messy and difficult to clean, special hawk-beak shaped tools were used to dry cut the aluminum block with a continuous flow of air on the metal surface. The structures obtained using this process were of comparable quality. Metal cutting tools are usually of smaller lengths compared to polycarbonate cutting tools.

CNC machining processes and SOLIDWORKS designing are always to be done with the tool restrictions such as tool length, tool diameter, tool life, ease of handling the tools, etc., in mind. Accurate initial positioning of the tool spindle is essential in order to properly align structures onto the surface. The material block that is machined has to be placed flat on a thin plate over the work bench to prevent drilling into the bench and having a flat surface with zero inclinations will result in accurate height of structures machined out of the material block. It is also important to tightly secure the tools to the spindle to prevent wobbling or detaching of the tool while the operation is carried out. Finishing process is to be carried out once the bulk material is removed using the roughing process to get smooth structures with cuts devoid of debris or tool marks. In order to increase the longevity of the tools used for cutting polycarbonate/aluminum blocks, the depth of cut for each pass assigned for a tool is always less than half of the diameter of the tool. Any higher depth cut, it might lead to breaking of the tool tip or the tool itself or the tool is rendered blunt quickly.

Once the molds are cut using the CNC machining, the master is attached to the bottom part of the mold made of aluminum. The top part of the mold containing the rough structures is polished and then assembled using screws after accurately aligning the microchannels structures with their counterparts on the polycarbonate mold.

3.3.2 CNC Machining of sensor holders

Two types of sensor holders were fabricated with the help of CNC machining process: polycarbonate sensor holder and aluminum sensor holder. As their name suggests, they were cut out from polycarbonate materials and aluminum block respectively. Sensor holder were cut in a similar manner compared to the mold systems as explained earlier. Since the footprint of both sensor holders are small, every step of cutting required extra attention to detail and accurate alignment became important. The structures of polycarbonate sensor holder were cut with relative ease when compared to the aluminum sensor holder. Aluminum sensor holder structures were really small and intricate and, in addition the tool length restrictions of the hawk-beak shaped cutting tools made it even more difficult to cut them out with precision and proper tolerance. Once most of the structures were cut, the deeper holes were drilled out manually with the help of drilling machine and drilling tools.

3.3.3 CNC Machining of multifunctional pipette mold systems

The multifunctional pipette mold systems were cut out in a similar fashion and with similar precautions as the mold system for microfluidic chips. But these systems required even more attention towards the alignment while cutting the structures on the back part of the mold after finishing the front part of the mold. CNC machining of multifunctional pipette mold systems helped improve by making finer tweaks and adjustments to the machining process of mold system for microfluidic chips.

3.3.4 Fabrication of multifunctional pipette holders

The multifunctional pipette holders had complex structures and moreover requires flexible finger-like structures. This made me rely on 3D powder printing using polyamide (Nylon) as material, which gave the most accurate structures.

3.4 Polishing of the mold

The polycarbonate mold after machining is semi-transparent in nature. This obstructs the view while aligning the mater with the structures. The first step involves mechanical polishing. It is a technique of smoothing of a surface using mechanical tools (polishing gun) and abrasives.

Abrasives such as sandpaper was used to remove deeper groove cuts made by the tools during CNC machining. Wax polishing was carried out in order to eliminate

lighter grooves made by the tools, and fine mesh 1200 sandpaper in some cases. This is a very tedious procedure which is to be done before resuming process called vapor polishing which makes the material surface transparent. If mechanical process is not done, vapor process still makes the surface transparent but the groove cuts made by the tools still remain.

Vapor polishing is implemented on the surface with a help of a solvent in order to polish the surface, and to obtain a transparency which is important for aligning the old surface. A component is exposed in this case to a solvent vapor, causing the surface to flow, thereby improving the surface finish. This method is often used to return clear materials to optical quality finish after machining. It works well in the intricate internal features of components. Plastics that respond well to vapor polishing are polycarbonate, acrylic, polysulfone, PEI, etc.

The solvent used in this process is methylene chloride (CH_3Cl). Methylene chloride is taken in a pressure-safe container with a perforation at the top, which is then gently heated until it turns to vapour. The vapour melts the top surface briefly upon exposure, and is thus smoothing it. Methylene chloride is not flammable, but toxic, and is to be handled with care. It is also to be noted that extended exposure of the polycarbonate again affects the transparency of the surface. The surface structures are slightly disfigured due to extensive melting and thus reducing the clarity of the surface. Typically, a quick, short and fast exposure gives the best results.

3.5 Device Fabrication

3.5.1 Fabrication of a SAR sensor

The SAR sensor is fabricated using a common photolithography process in the clean-room. The fabrication process of SAR sensor is illustrated step-by-step in figure3.10. The first step is to take a wafer and clean it with rem-400, IPA and water to make it particle-free. Dehydration bake of 5mins on a hotplate at 190°C is done to rid the surface of any water. It is to be noted that Teflon coated tweezers is used to handle the wafer. A sacrificial polymer layer of LOR3A is spin-coated at 3000rpm for 45sec and is baked for 5mins on a hotplate at 190°C. A lift off process is used to get well-defined structures. S1805 resist is spin-coated onto the wafer at 3000rpm for 30sec and baked on hotplate at 110°C for 2min. By using 2 layers of material it is possible to create a negative profile (undercut) which is to get better definition of the features. Direct-Writing (DWL) series of laser is used to expose the resist with Int 45, Foc 45, Trans 100. The exposed structures are developed in MF CD-26 developer for 50sec and the undercuts obtained are similar to figure 3.11.

A descum process is used to remove residual photo resist in trenches. The metals are deposited onto the structures using an evaporation technique, and layers deposited are titanium (Ti) 25nm thick, gold (Au) 260nm thick and again titanium of 15nm. A lift¬off technique is used by immersing in Shipley 1165 remover with sonication.

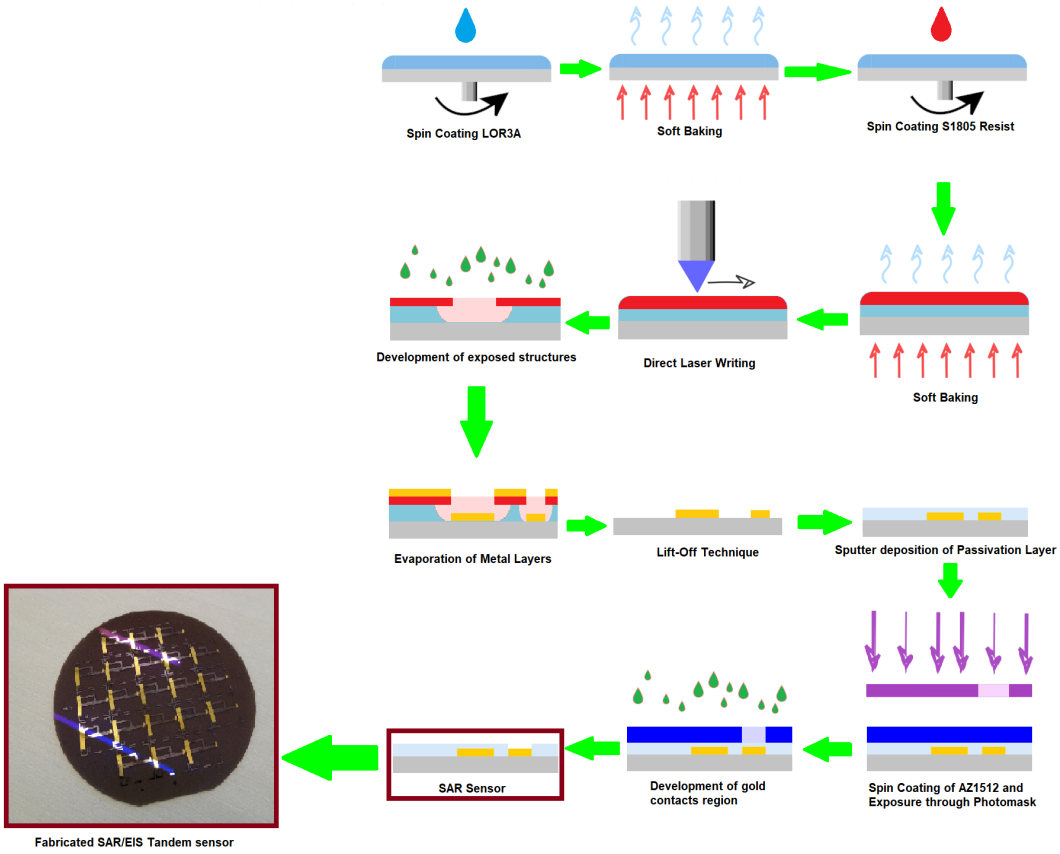

Figure 3.10: Cleanroom fabrication process of SAR sensor

Figure 3.11: Undercuts obtained in a two-layer process (Image from http://lnf-wiki.eecs.umich.edu).

The wafer is then cleaned with REM-400, IPA, and DI water and then sputter coated with 100nm of SiO2. The resist AZ1512 is spin-coated onto the structures, baked for 30sec, exposed using a photomask or laser writing with UV-light (365 nm or 405nm), developed in MF-CD26, and rinsed in DI water before plasma etching out the regions of gold contact pads using the Oxford Instruments ion etching tool. Another layer of AZ1512 is coated on the finished surface to protect the structures underneath it while carrying out the dicing process to cut the wafer into individual SAR sensors.

In one wafer, a maximum of 21 15x15 SAR sensor dices can be fabricated using the above mentioned process of lithography. In most of the cases SAR sensors obtained from a single wafer is less than 21 sensors. This is due to the fact that structures in some regions of the wafer remain under-developed or over-developed. Despite this, the process is quite cost-effective as multiple sensors are fabricated in a single

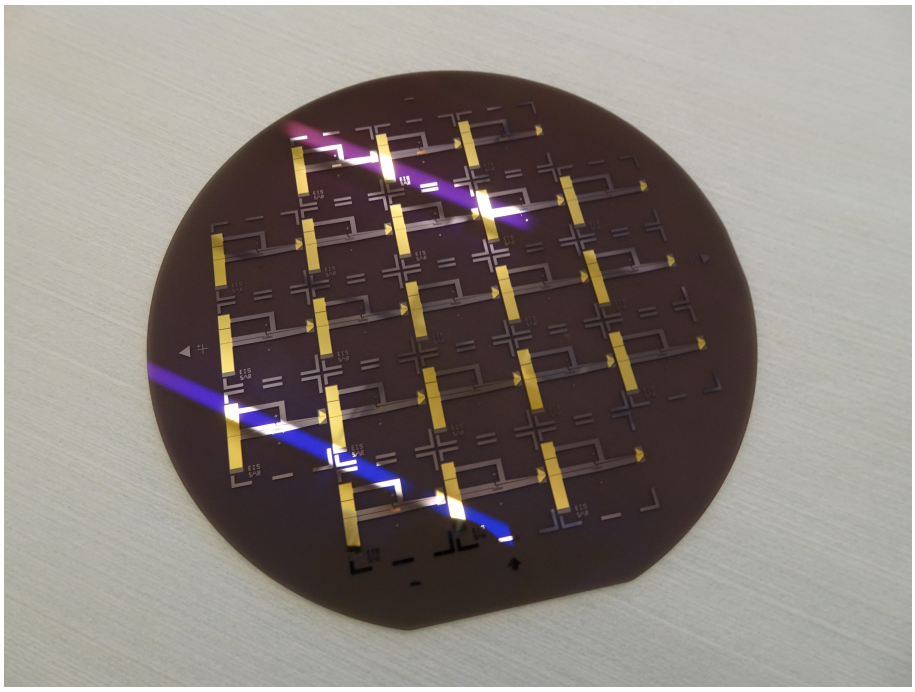

Figure 3.12: Fabricated sensor wafer with 21 SAR sensors

process. Figure 3.12 shows the fabricated sensor wafer with 21 SAR sensors.

3.5.2 Fabrication of microfluidic chips

3.5.2.1 Photolithography

Photolithography is a microfabrication patterning technique in which a photosensitive polymer is selectively exposed to light through a mask, leaving an image in the polymer that can then be dissolved to provide patterned access to an underlying substrate. This fabrication process is used to fabricate the master wafer consisting of microfluidic circuit design.

Figure 3.13 gives the entire fabrication procedure for microfluidic chips. It involves: Fabrication of the master wafer, passivation of the master, PDMS preparation and fabrication of microfluidic chips. The first six steps of the diagram details the processes involved in fabrication of the master wafer and the last three processes gives fabrication of microfluidic chips with the help of microfluidic mold system.

The raised structures on the master are fabricated in SU-8 which is an epoxy-based negative tone photoresist [28]. The main steps of the photolithography process are illustrated in figure 3.13. The master wafer to be used is cleaned and is spin-coated with SU-8 2035. The thickness of the photoresist depends on the design of the microfluidic channels, as it will determine the height of the channels. The SU-8 is then pre-baked in two steps, at 65°C and 95°C to make sure the solvents evaporate [28]. Through a mask, the resist is exposed with UV-light at 365nm in the Suss semi-automated mask aligner MA 6. As SU-8 is a negative photoresist, the exposed

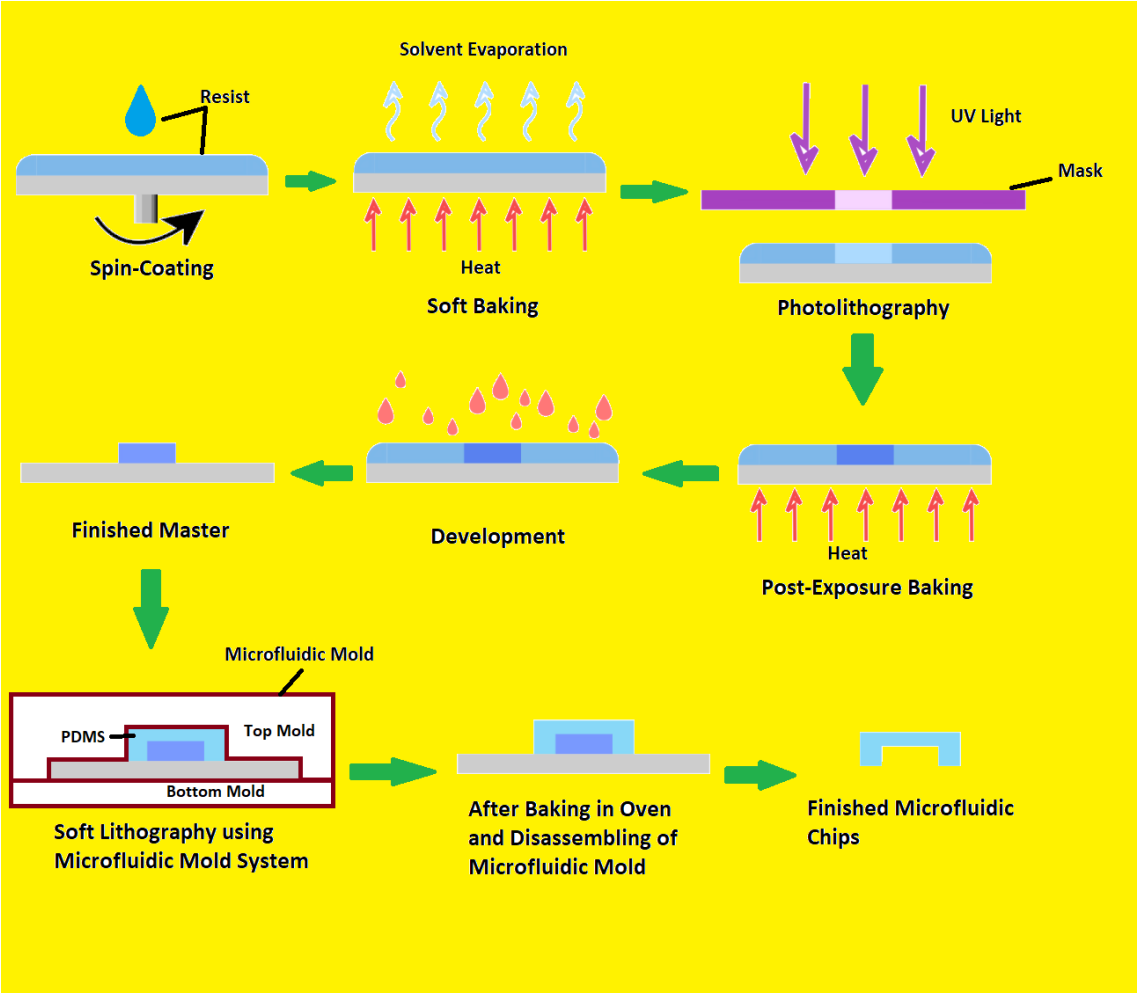

Figure 3.13: Fabrication process of Microfluidic Chips

regions are cross-linked, and patterned regions are obtained through the mask. The wafer is then post-baked so that the cross-linking process, which started during exposure, is completed. This is done in two steps, at 65°C and 95°C to minimise generation of stress in resist. SU-8 is then developed in mr-Dev 600 developer and rinsed in IPA to remove all the unexposed resist while leaving behind only the desired structure on the substrate . The substrate is then O_2 plasma etched using the PlasmaTherm Reactive Ion Etcher (RIE) to rid the surface of any remaining unexposed resist, and the wafer is hard-baked at 200°C. This results in a finished master wafer with the microfluidic channels. The master is then passivated before using it in the mold.

3.5.2.2 Soft Lithography

Soft lithography is just a term used for several different fabrication techniques that all make use of some type of soft polymer. PDMS is one such soft polymer that is being used for fabricating microfluidic structures.

PDMS preparation involves manual mixing of PDMS and curing agent in the ratio

of 10:1. Then the mixture is de-gassed (removal of air bubbles) using a vacuum/de-gassing chamber. The total volume of PDMS mixture to fill the entire mold is 44g (40g of PDMS and 4g of curing agent). Now the passivated master wafer, which is attached/glued to the bottom part of the mold, and the mold top are aligned and assembled. The PDMS mixture is poured into the mold. Once the mold is completely filled, a few ml additional PDMS is poured into the mold. This is essential because when the PDMS cures in the mold while the mold is left in an oven at 65°C, PDMS shrinks. The extra PDMS compensates for the shrinking. After 1.5 hours, the mold is removed from the oven and cooled until it reaches room temperature. Then, the mold is disassembled and the PDMS chips are obtained.

It is to be noted that if PDMS is heated at even higher temperatures, the curing time is shortened, but the the elasticity (rubbery feeling) of the PDMS is also reduced.

3.5.2.3 Passivation of the wafer

Passivation involves creation of an outer layer of material that is applied as a coating, created by exposing the surface to a surface-reactive chemical in vacuum. It is important to properly passivate the wafer as it prevents strong adhesion to the PDMS to the master after the curing process is complete. This protects the wafer from breaking when the mold is disassembled after the curing of PDMS is done.

For passivation, the wafer is kept with 0.1m1 dichlorodimethylsilane in a vacuum chamber, e.g. a dessicator. The chemical evaporates and coats the surface of the wafer as a thin molecular film, and is thus protecting the wafer unwanted adhesion. It is to be noted that only the master wafer, but not the SAR sensor, is passivated before use.

3.5.3 Oxygen plasma treatment and sensor-chip bonding

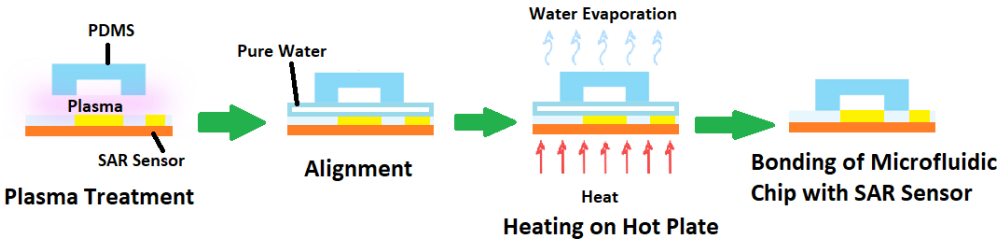

Figure 3.14: Plasma Bonding of SAR Sensor

PDMS has a number of properties which make it favourable for its use in microfluidic devices: bio-compatibility, low cost, easy processing/molding, transparency, chemical inertness to polar solvents, etc. Similarly, oxygen plasma treatment has also become an irreplaceable technique to seal the PDMS microfluidic channels.

For the PDMS surface and SAR sensor surface to be bonded, they are exposed to oxygen plasma in a plasma generating device (Atto plasma cleaner, diener electronic). After 3-5 cycles of pumping oxygen into the chamber, the plasma generator

is switched on for one minute. On both substrates, the treatment is effective at removing hydrocarbon groups (C_xH_y) leaving behind silanol groups on the PDMS and OH groups on the sensor substrate respectively. This allows strong Si–O–Si covalent bonds to form between the two materials once they are bonded to each other. Water molecules are released when this bonding happens and they are removed by heating up the SAR sensor on a heating plate.

Accurate alignment of PDMS microfluidic chip and SAR sensor is of utmost importance in order to obtain a functioning sensor assembly. The microfluidic containers must align onto the reflector gratings while the protective air cavity must overlap IDT in-between the ground and EIS as shown in figure 3.8. This alignment is achieved while continuously observing through an optical stereo microscope. As aligning at microscale takes a while, MilliQ water is deposited on SAR sensor surface after plasma treatment to delay the bonding between SAR sensor and PDMS microfluidic chip. Once the alignment is satisfactory, the sensor is subjected to heat of 35°C on a hot plate for one hour so that water begins to evaporate. There are chances that our alignment shifts due to evaporating water at this stage. If necessary, alignment changes are done and the sensor is baked at 50°C for a couple of hours to obtain perfect bonding. Figure 3.14 shows the procedure of plasma bonding followed and figure 3.15 gives detailed schematics of plasma bonding chemistry.

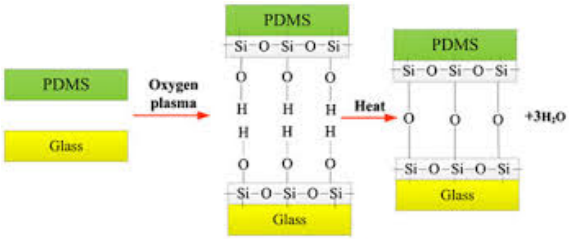

Figure 3.15: Schematics of plasma bonding chemistry [23]

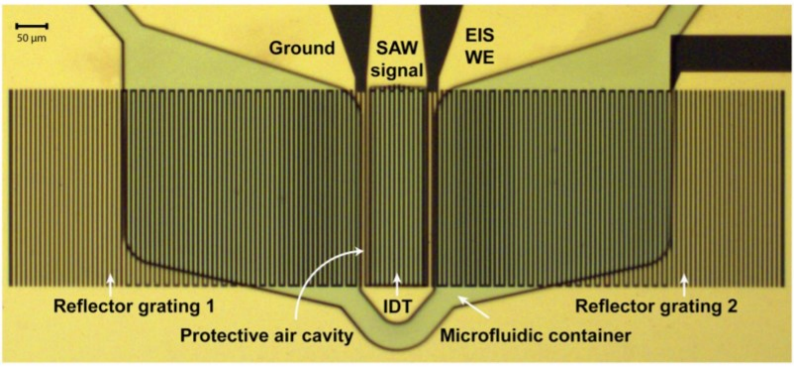

Figure 3.16: Optical microscopy image of microfluidic chip bonded onto a SAR sensor surface with proper alignment [27]

3.5.4 Sample preparation

As there has been no previous measurements done using the SAR sensor at higher temperatures, the system was tested with milliQ water. Then, to measure the

viscosity, a simple but viscous fluid had to be selected. Thus, sucrose ($C_{12}H_{22}O_{11}$) was chosen.

First, 20.0 g sucrose was weighed and dissolved in27.5 g of milliQ water to prepare a stock sucrose solution. Hence,

Mass of sucrose crystals = 20.0g
Mass of milliQ water = 27.5g
Mass density of stock solution = $\frac{Mass\ of\ Sucrose}{Mass\ of\ Sucrose+Mass\ of\ milliQ\ water} = 42.08$

Solutions of mass percentage of 5%, 10%, 15%, 20%, 25%, 30%, 35% and 40% of stock solutions were prepared and labelled as sample 1, sample 2, sample 3, sample 4, sample 5, sample 6, sample 7 and sample 8 respectively. The total volume of these solutions prepared were of 2ml each. The mass and volume of milliQ water used to dilute the stock solutions were recorded. The solutions are then filtered using 0.2μm sized micro-filters and degassed using sonicator for 15-20 mins. This eliminates solute particles and micro-bubbles in the sample solutions. Now the solutions are ready to be injected into the sensor. It is to be noted that filtration of the samples once a week are necessary to remove the microbial contamination and the samples are to be stored in the refrigerator after the measurements at the end of the day.

No	Concentration of sucrose (Mass %)	Volume of milliQ water (ml)	Volume of stock solution (ml)	Mass of milliQ water (g)	Mass of stock solution (g)
0	0	2	-	-	-
1	5	1.762	0.238	1.6968	0.2772
2	10	1.525	0.475	1.447	0.5491
3	15	1.287	0.713	1.2614	0.822
4	20	1.049	0.951	1.02	1.1216
5	25	0.812	1.188	0.794	1.347
6	30	0.574	1.426	0.54	1.6314
7	35	0.337	1.663	0.336	1.892
8	40	0.099	1.901	0.1	2.166

Figure 3.17: Table displaying the details of the samples prepared

3.5.5 SAR sensor measurement platform

The SAR sensor measurement platform that I developed is used to study fluid properties of viscous solutions. Here, the of SAR sensor measurement platform is explained in regards to viscosity-temperature measurements.

Firstly, the injection system is positioned in load position and a bottle of milliQ water is degassed using a sonicator for 5-10 mins. The degassed water bottle is fixed to a stand and a tube is connected from the bottle to the inlet port of the injection system. A pressure tube is also connected from the pressure pump and the bottle. The sensor is placed in the frame of the sensor holder and covered with the top portion of the sensor holder. The top portion of the sensor holder is connected to the Mini-VNA device, which is also connected to a PC. The bottom portion of the sensor holder has a thermocouple and a ceramic heating plate, which are connected

to the temperature controller. Supply tubes are connected from another port of the injection system to one of the fluidic ports of the sensor through the top lid of the sensor holder. The other fluidic port of the sensor is connected via another tube in a similar fashion to a bottle which collects the fluid exiting the sensor. The outlet port of the injection system is connected to a waste-collection bottle. Now the entire system is ready to run.

The pneumatic pressure pump is switched on manually, and the temperature controller is also turned on. It is important to run fluid through the sensor in this system initially at room temperature, to prevent expansion of air bubbles and col-lapsing of microfluidic channels. Then, the Mini-VNA script is run in MATLAB, and the pressure pump software is turned on. 150mbar of pressure value is en¬tered into the pressure pump software and the flow is turned on. Now, water is seen exiting into the bottle through the tube. This will provide verification that the tubes are connected properly into the microfluidic channel system of the sensor. The MATLAB program used to run the Mini-VNA starts displaying/recording the measurement values. After sometime, the temperature of the sensor system is increased as per the requirement, and the water is run through the sensor system continuously until the temperature of the sensor system has stabilized and the flow signals on the monitor present a stable baseline. This proves that the SAR sensor as well as the entire measurement system are ready to inject samples that I had earlier prepared.

Firstly 40μl of milliQ water is injected into the injection system after the lever of the system is turned to inject mode. After injecting, the "save measurements" reading option is enabled on the monitor screen which stores the data by converting the measurements shown in graphical format to text file .txt. Thereafter, the lever of the injection system is turned to load position which makes the injected sample into the sensor. Since 20μl is the sensor capacity, the rest of the sample is collected in the waste bottle. Since, milliQ water was supplied, there should not be any change in the measurement signals. Once, no change is observed sample 1 can be injected.

Sample 1 is of the lowest sucrose concentration whereas sample 8 has the highest sucrose concentration. A microsyringe is used to inject 40μl sample 1 into the injection system following the same procedure as explained above. Once the sample is injected, the pre-existing data has to be saved before turning the lever back to the load position. This has to be quick to prevent blockage of the flow which causes unwanted change in all the measurements signals. The microsyringe is then washed with milliQ water before injecting the next sample. This is to prevent cross-contamination of samples. This process is followed until all the samples are tested and the changes in the signals are noted to be as expected or predicted.

After testing all the samples, the entire system including the sensor is flushed with milliQ water to remove all the traces of the sample in the system as well as sensor. This can be seen in the measurement signals that is generated during this process. The miniVNA and pressure pump programs are then switched off. The system can also be left in the standby position. This position maintains a minimum water flow in the system but the input bottle has to be refilled and waste bottle emptied before

leaving the system in the standby position.

It is important that while connecting the tubes to the sensor, strong force should not be applied, due to the risk that the sensor might break due to the unnecessarily high force. It is also important to observe any leakage in the system or blockage in the tubes. Continuous observation of the outlet tube is necessary to ensure proper flow in the sensor.

4

Results and Discussion

This thesis work was carried out to develop a seamless repeatable fabrication process of microfluidic systems and develop a measuring platform for viscosity-temperature measurements. The fabrication process of microfluidic systems led to development of mold systems. Developing a measuring platform also included designing and fabrication of sensor holders. The designing part has also been completed for successful integration of multifunctional pipette with SAR sensors. Viscosity measurements at different temperatures with the Mini-VNA were carries out to test the measurement platform.

4.1 Microfluidic Mold system

The microfluidic mold system was developed for easier handling and improved flow of PDMS during the process of casting, with facilitated alignment and assembling of the mold system, as well as disassembling of the mold system and effortless handling of fabricated microfluidic devices in mind.

Three microfluidic mold systems have been designed, fabricated and used throughout the thesis for the fabrication of microfluidic chips, and multifunctional pipettes. The designing, CNC machining and the use of the mold systems are explained in detail earlier in methods section of the thesis. The intention is to use PDMS as comfortably and safe as possible, since PDMS is quite sticky and contaminates surfaces. The waste of larger amounts of PDMS should also be prevented.

The main focus is on fabricating multiple microfluidic chips at a time, while the con¬cept of mold system has been extended to fabrication of similar microfluidic devices. The adaptation of this concept to fabricating sensor molds as well as multifunctional pipettes led to development of special mold systems. These complex mold systems helped guided the PDMS flow in the molds without waste and spilling. The most important result was successful fabrication of bubble-free microfluidic devices. A U-Flow system has been developed to meet the requirements. The U-Flow system makes injection of PDMS unnecessary. The polymer can be filled from its preparation container, and air bubbles are transferred out efficiently.

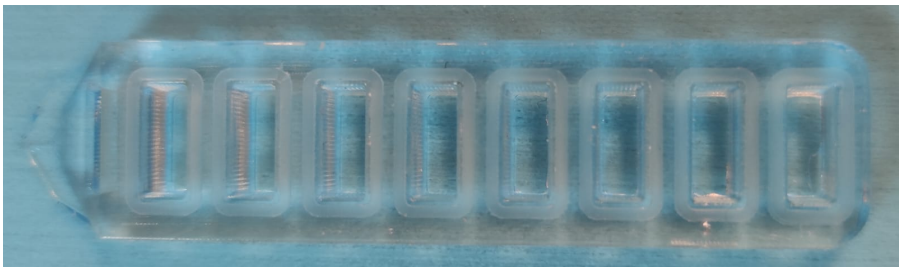

Figure 4.1: Fabricated multifunctional pipette using the pipette mold system. The large dimensions make it suitable for future integration with the sensor chip.

Figure 4.2 shows the mold system developed for fabricating microfluidic chips. The microfluidic mold system has to be assembled with proper alignment as explained in the figure. The white highlighted region of the mold has to perfectly align with the white highlighted region of the master wafer of the other part of the mold system. To help in accurate alignment, we have alignment marks on the master wafer, and polishing of the mold surface helped generating a transparent surface. In between the parts of the mold, a rubber ring is used for sealing, which protrudes by 0.2-0.5mm. This also helps to prevent excessive force on the master and prevent breaking of the master wafer.

In this mold PDMS flow occurred due to gravity. This makes PDMS flow possible into covering all cavities evenly. Rounded corners prevents entrapment of air bubbles inside the mold system and regular channel connections between every microfluidic chip make it possible for a well-directed flow.

Disassembly of the mold system is also equally important,. It was observed that, if the mold system is disassembled while it is hot or even warm, the master wafer might lift off from the bottom plate, and break in the process. It is also seen that once the mold system is completely cooled to the room temperature, the adhesion of the master to the adhesive tape on the aluminum bottom part is high, and the master wafer is perfectly separated from the solidified PDMS.

Mechanical polishing of the mold top is justified, as it will rid the surface of deeper tool indentations and shallow scratches. During chemical (vapor) polishing it was noticed that deeper tool indentations cannot be eliminated with chemical polishing, and need to be removed prior to vapor exposure. The use of chemical polishing gives sufficiently transparent surfaces, which supports greatly accurate alignment of the structures. The microfluidic chips can be viewed directly under the optical microscope while aligning. A drop of silicone oil can alternatively be used on the PDMA top surface to establish transparency, but it is best avoided since it creates the risk of seeping into the sensor through the port holes on the chips, which renders the SAR sensor nonfunctional.

Overall the fabrication of microfluidic chips using the mold system is found to be useful, clean and efficient. The aim of fabricating multiple well aligned microfluidic chips in a single process was accomplished. The SAR sensors with microfluidic

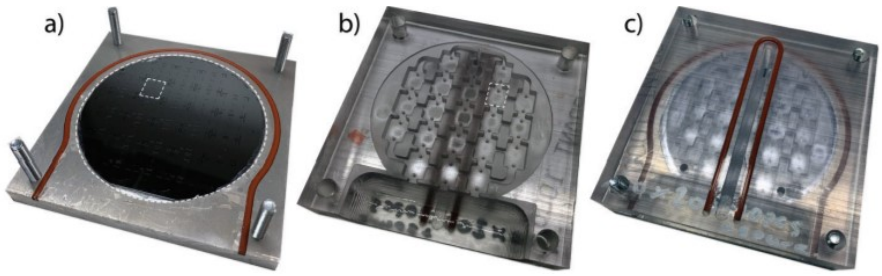

Figure 4.2: Final functioning microfluidic mold system. a) Bottom part of the mold with master wafer glued and white square indicated. b) Top part of the mold with another white square indicated. c) Assembled mold system with both the white squares aligned together.

chips obtained are of very good quality and the high accuracy in their alignment is repeatedly achieved.

4.2 Sensor holders

Several holding structutres/enclosures have been fabricated: polycarbonate sensor holder, aluminum sensor holder, aluminum sensor holder with thermocouple and heating element, and multifunctional pipette holder.

Designing and fabricating a multifunctional pipette holder provided true in-depth understanding of the fabrication process. The pipette holders were very detailed in design and at the same time really simple to use. It did not require any screwing mechanism to tighten the grip on the pipette to create vacuum over the well. The finger-like structures provided with two ways of locking and unlocking the sensor and thus extending the life of the holder itself. The pipette holder gave me the knowledge of the flow channels and ability to efficiently utilize space on to maintain a small footprint. This helped me for the second step: the development of the sensor measurement holder.

The aluminum sensor holder required complete re-design to overcome the problems faced by the polycarbonate sensor holder. This led to a composit design with an additional PCB, which has replaced the previously used soldered copper wires. The use of a PCB improves the issue of impedance losses. The standard aluminum sensor holder had much better isolation from external interference than the polycarbonate sensor holder, and the measuring signals had better stability due to this. Then an aluminum sensor holder with thermocouple and heating element was designed and fabricated. This latest holder provided control over the temperature of the system, and has features to aid in accurate positioning of the sensor in the holder. It is observed that positioning of a ceramic heating element 2-3mm below the sensor with thermocouple have led to sufficient heat transmission to the sensor while heating, precise temperature reading and precise temperature maintenance over longer periods of time. The goals of good thermal and interference isolation, integration of more

useful modules (temperature control module in this case) into a smaller footprint by design and fabrication of a suitable sensor holder was successfully achieved.

4.3 Sensor measurement platform

This measurement platform, consisting of sensor holder, VNA, temperature control unit, pump and injector has been used to perform viscosity-temperature studies of fluids in microscale. Other currently available equipment for viscosity-temperature studies of fluids is bulky, takes longer time for fluid studies and, most importantly, requires larger volumes of fluid samples. There are distinct instances in life science research where expensive samples have to be studied for faster interactions. These samples can be measured in real-time using the new measurement platform, since the amount of sample required is only $40\mu1$. The fluid capacity of the sensor is $20\mu1$, whereas the remaining $20\mu1$ is waste collected from the injection system, which is currently unavoidable but may be further reduced in a fully integrated microfluidic system.

4.3.1 Summary: Advantages of new measuring platform over older systems

- The latest generation of the measuring platform has an easily usable and accurate injection system which requires 40μl of sample injection while 20μl is collected as waste from the injection loop.
- External interferences are strongly negated with the use of aluminum sensor holder.
- The measuring platform has an accurate temperature control system. The newest design of sensor holder houses a ceramic heating element and a thermocouple which are useful in conducting viscosity and temperature studies of fluids.
- The entire measuring platform is robust, portable, and easy to use. It is also uncomplicated to correct intermittent problems that might arise during measurements.
- Finally it is a setup that can truly support the multi-parametric sensing capability of the sensor.
- The platform can be easily dismantled and is easily upgradable for conducting advanced studies in the future.
- The measurements are repeatable and accurate and the flow loss in the system can be controlled.
- It can finally support real-time (live) measurements and can be used in point-of-care testing as well.

I have used this measuring platform to perform viscosity-temperature studies with the help of a simple model solution, such as sucrose, in order to performance test the measurement platform.

It is noted that this measurement platform, though advantageous, has some flaws which can be corrected in the future iterations. Flow-related issues were persistent due to the use of flow tubes that connects the injection system and the outlet bottle with the sensor and the sensor holder which is this system's weak link. It is observed that the sweet spot achieved while plugging the fluid ports of the sensor with the flow tubes is lost frequently and has to be manually adjusted in the same port if the measurements are being taken. The flow tubes also get clogged with waste relatively easily, thereby giving wrong measurement signals, and also depositing debris into the sensor. This cannot be solved until the flow tubes are changed to a new one.

Possible solutions to the flow issues experienced is to use some sort of insertions in the flow ports that guide the flow tubes in and out of the sensor through the holes on top portion of the sensor holder. This might be a only temporary fix to the flow problems.

Another plausible solution is to integrate the multifunctional pipette with the SAR sensor and use the reverse mechanism of the pipette to forcibly push the fluid from the wells of the pipette into the microfluidic channels. The sample is then directed to the sensor. This can successfully overcome all the flow issues still faced in the current system. Overall the aim of developing a measurement platform for SAR sensor to conduct viscosity-temperature studies was successful. Initial development work has been done to facilitate the integration of a multifunctional pipette body with the SAR sensor.

4.4 Repeatability of the SAR sensor

With the use of the new measuring platform, the sensor measurements are found to be repeatable not only at room temperature but also at higher temperatures.

Using the samples I prepared of sucrose solution of varying concentrations, I have got two sets of measurements for each temperature of 25, 30, 35, 37 and 40°C. The data measurements give me the values for conductance (G mS), resistance (R Ω), resonance frequency (f_R MHz), anti-resonance frequency (f_G MHz) and dissipation (D) over time (t seconds). I analysed the data with the help of ORIGIN PRO to do signal smoothing, baseline correction and integrated the peaks which is the change in the signal when a sample is introduced. The data analysis gave me the area of the peaks and frequency shifts of G, R, f_R, and f_G which I have plotted into the graphs against concentration of the sucrose solution (calibration curves).

Figures 4.3 and 4.4 are the plots of two sets of data I obtained for G, R, f_R, and f_G at lower temperatures of 25 and 30°C. It is seen that the values of conductance and anti-resonance frequency at 25 and 30°C have similar values with a few orders of magnitude difference which is to be expected as new SAR sensor was used for every

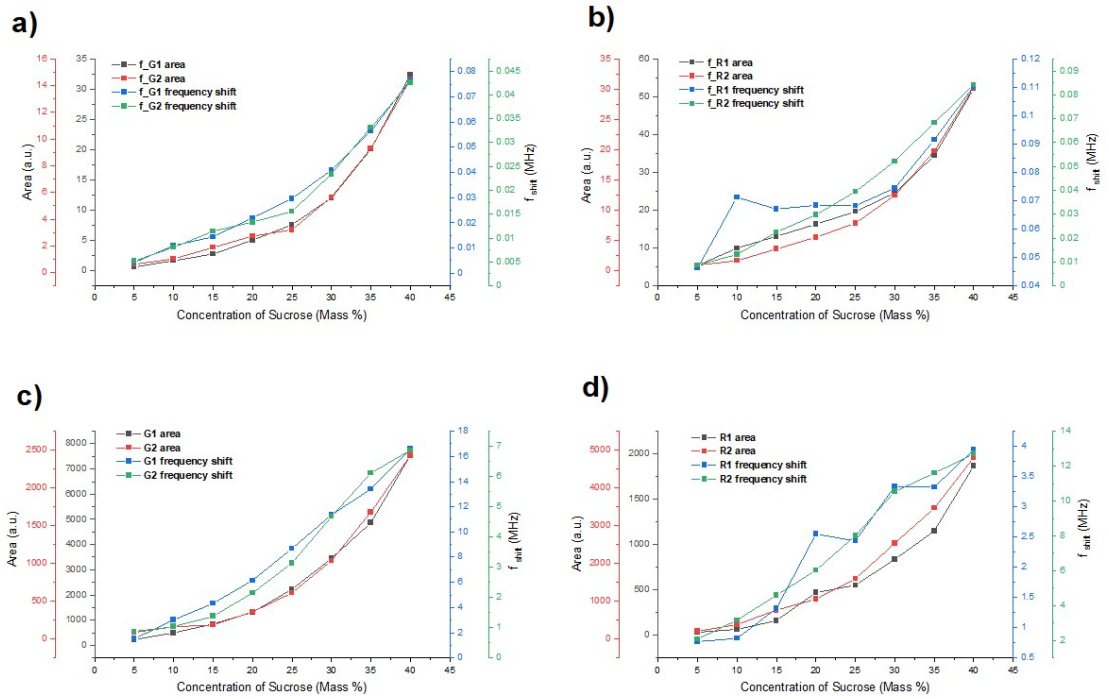

Figure 4.3: Repeatability tests at 25°C. a) Anti-resonance frequency vs. concentration. b) Resonance frequency vs. concentration. c) Conductance vs. concentration. d) Resistance vs. concentration.

set of measurement. Even though I used two sensors for measurement, the values are found to be repeatable. Comparable sets of values for resonance frequency and resistance at 25° and 30°C were obtained, as seen from the figure.

It can be inferred from the figures that the performance of the sensor is acceptable at room temperatures, since the areas and frequency shifts of all the measuring signals are similar.

Figures 4.5 and 4.6 are the plots of two sets of data I obtained for G, R, f_R, and f_G at lower temperatures of 37 and 40°C. I got satisfactory results even at higher temperatures. It is seen that the area of the peaks and frequency shifts of G, f_R, and f_G are quite repeatable with a slight difference at 37°C. The area of the peaks of the resistance values appears to be very similar, whereas the frequency shifts of both sets of data does not seem to follow a pattern at all. A possible reason for such a behavior could be sudden and frequent changes in the flow rate of the sample into the device. Further investigations are required.

Even at 40°C, the measurements show, G and f_G that the conductance and anti-resonance frequency values are least affected by the rise in temperature. The areas of the peaks of f_R and R are similar between series, but the frequency shifts of the peaks of R and f_R are apparently drastically affected causing such a random change in the values. Hence, while observing the real-time measurements, it is best

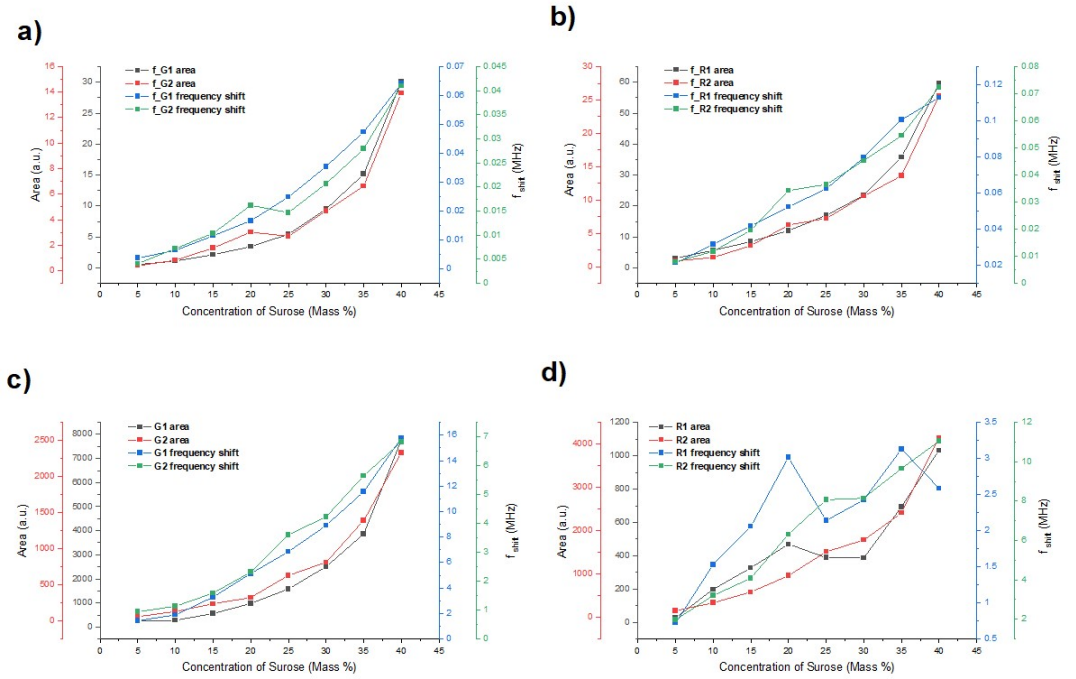

Figure 4.4: Repeatability tests at 30°C. a) Anti-resonance frequency vs. concentration. b) Resonance frequency vs. concentration. c) Conductance vs. concentration. d) Resistance vs. concentration.

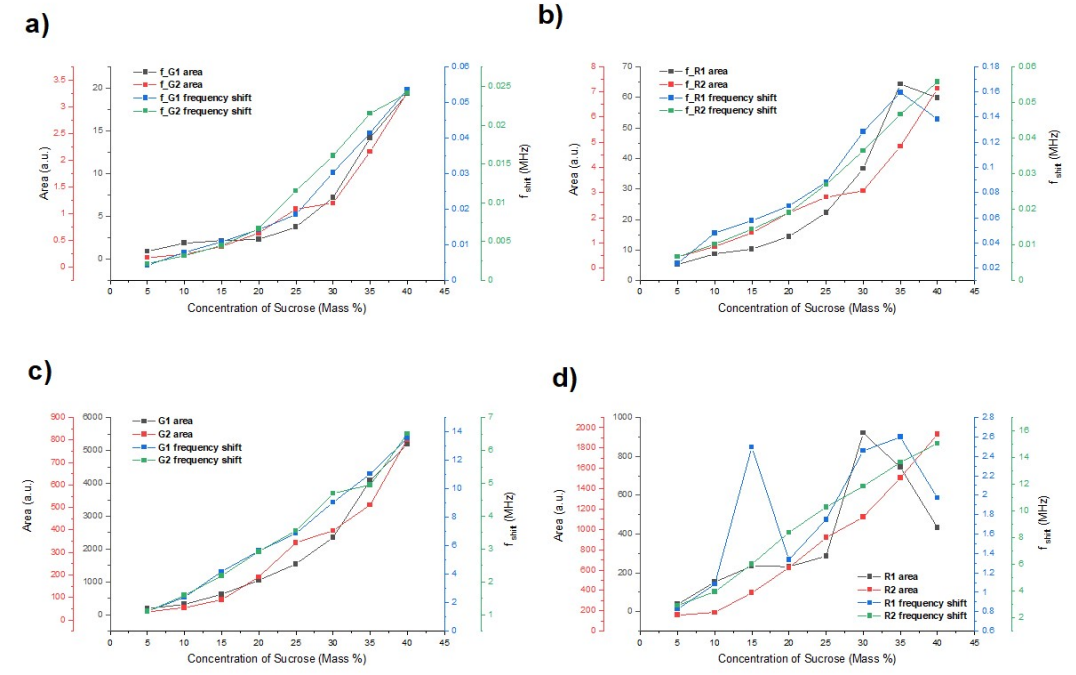

Figure 4.5: Repeatability tests at 37°C. a) Anti-resonance frequency vs. concentration. b) Resonance frequency vs. concentration. c) Conductance vs. concentration. d) Resistance vs. concentration.

to monitor the conductance values, as they give according to the findings presented here the most reliable values in the raw format, even at higher temperatures.

It can be concluded that the performance of the SAR sensor is satisfactory even at higher temperatures, and the repeatability of the sensor measurements is adequate. The system passed this initial test, but statistical evaluation with larger measurement series on different analytical systems should be performed in order to obtain quantitative data.

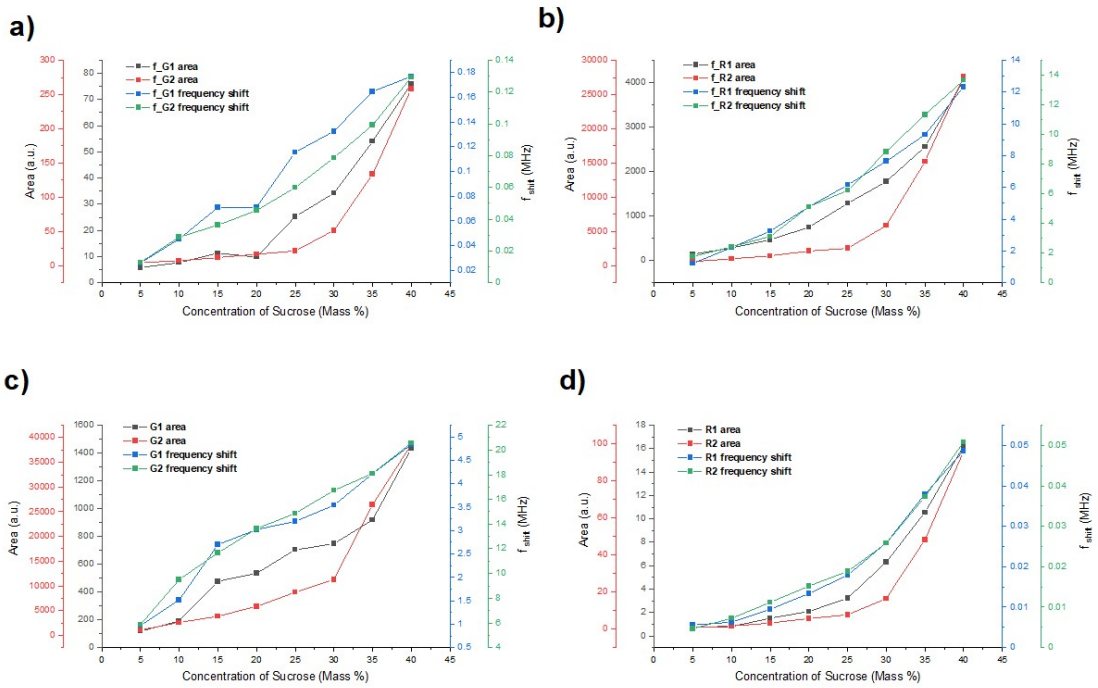

Figure 4.6: Repeatability tests at 40°C. a) Anti-resonance frequency vs. concentration. b) Resonance frequency vs. concentration. c) Conductance vs. concentration. d) Resistance vs. concentration.

4.5 Temperature studies

The anti-resonance plots show that there is a slow rise in the area of the peaks and frequency shifts initially for samples 1(5%), 2(10%), 3(15%) and 4(20%). Beyond sample 4 there is a sharp rise for sample 5(25%), 6(30%), 7(35%) and 8(40%). This indicates that higher the viscosity of the samples, stronger changes in the signals is observed. This trend is quite the same in all the measured signals (G, R, f_R, and f_G).

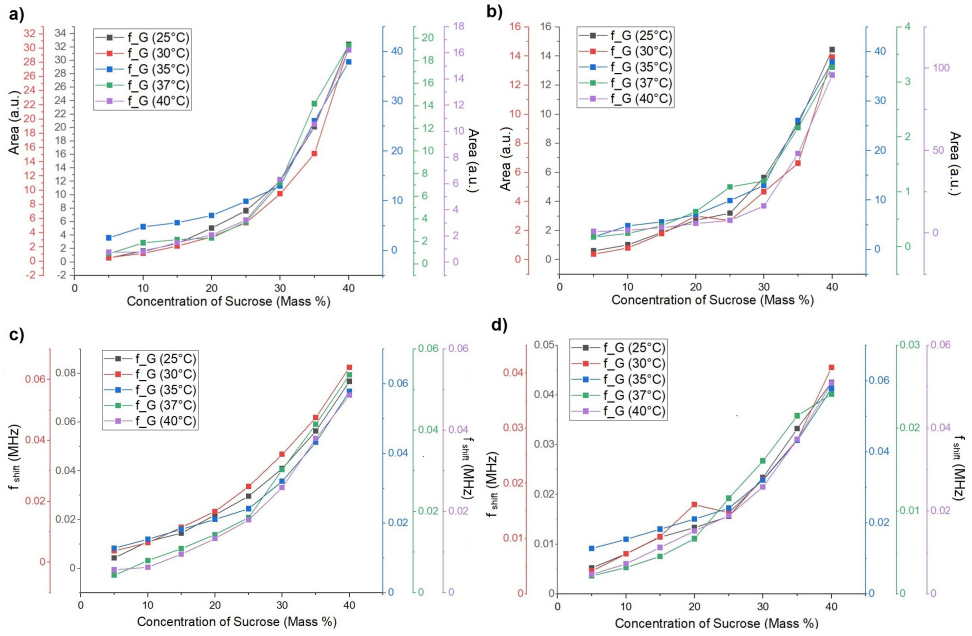

Figure 4.7: Anti-resonance plots for two data sets at different temperatures. a) set 1 area plots b) set 2 area plots c) set 1 frequency shift plots d) set 2 frequency shift plots

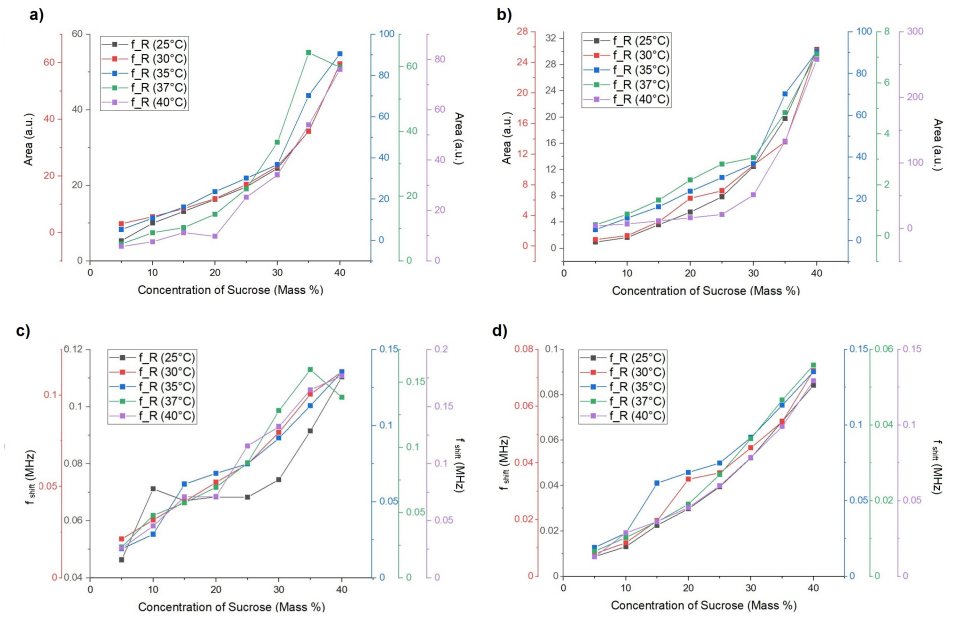

Figure 4.8: Resonance plots for two data sets at different temperatures. a) set 1 area plots b) set 2 area plots c) set 1 frequency shift plots d) set 2 frequency shift plots

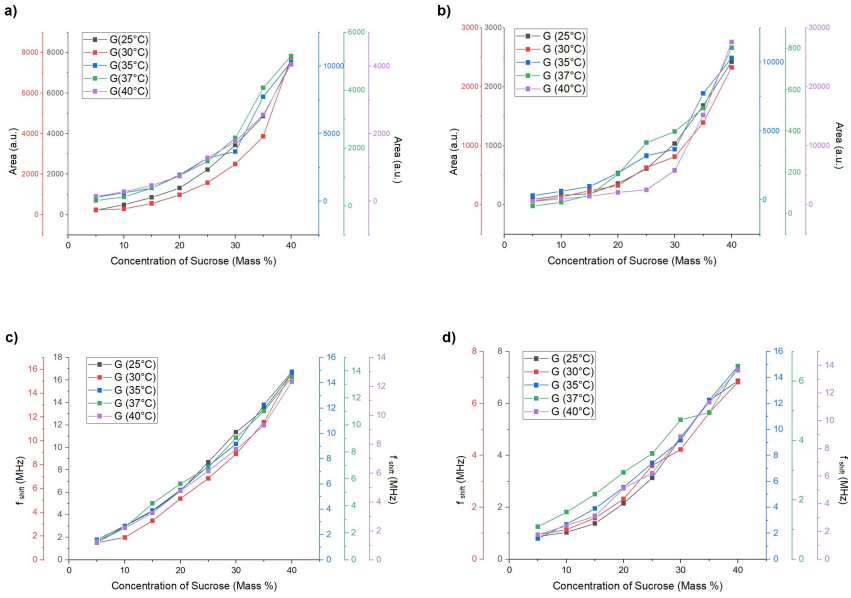

Figure 4.9: Conductance plots for two data sets at different temperatures. a) set 1 area plots b) set 2 area plots c) set 1 frequency shift plots d) set 2 frequency shift plots

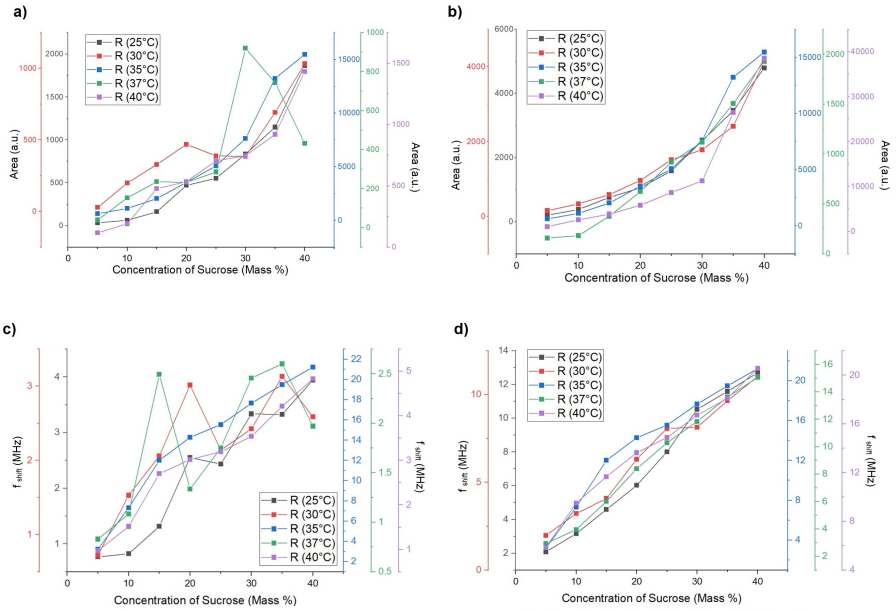

Figure 4.10: Resistance plots for two data sets at different temperatures. a) set 1 area plots b) set 2 area plots c) set 1 frequency shift plots d) set 2 frequency shift plots

It is repeatedly noted in all the plots of G, R, f_R, and f_G that the measured values at 40°C are lower in magnitude than those obtained at 37°C. This can be accounted to the fact that all biological processes are carried out at 37°C. There is currently no explanation of this behavior, and further studies are advisable.

4.6 Effect of temperature on change in frequency shifts

The data analysis of the two set of measurement signals was done and plots shown in figure 4.11 and figure 4.12 were obtained for the concentrations 5% and 40% respectively. It can be seen that the graphs are different for set 1 and set 2 data. This phenomena could not be explained during the short interval of time and requires extensive data analysis and interpretation that can also be a possible future scope of the thesis as it is very important to understand how much the values obtained are increased at a certain temperature for a fluid of specific viscosity. This temperature change can be subtracted automatically while recording real-time measurements for a more accurate set of data.

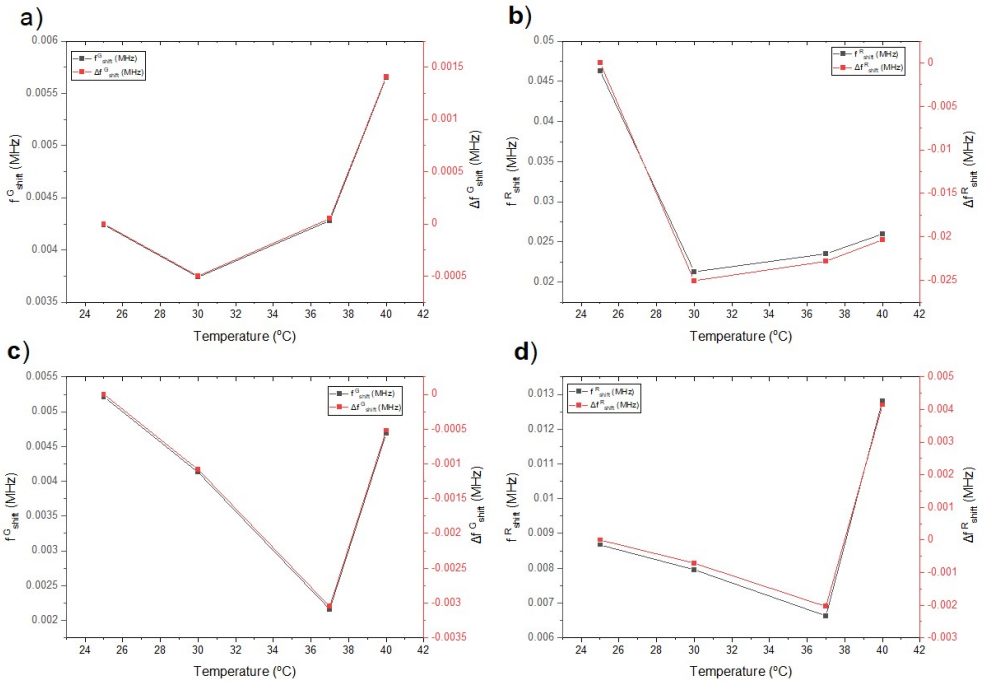

Figure 4.11: Change in frequency shifts vs temperature for 5% concentration. a) anti-resonance frequency shifts (set 1) b) Resonance frequency shifts (set 1) c) anti-resonance frequency shifts (set 2) d) Resonance frequency shifts (set 2)

If the change in frequency shifts at different temperatures for known fluid viscosities is successfully obtained and the results are repeatable, then an equation for change in frequency shift can be established for a specific fluid. Along with this equation and

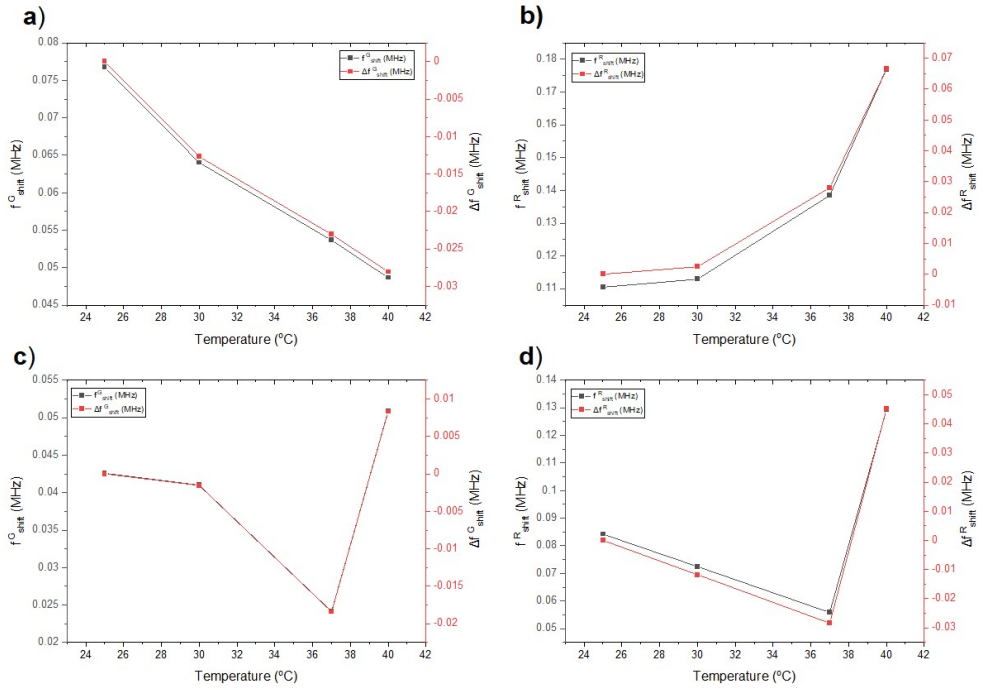

Figure 4.12: Change in frequency shifts vs temperature for 40% concentration. a) anti-resonance frequency shifts (set 1) b) Resonance frequency shifts (set 1) c) anti-resonance frequency shifts (set 2) d) Resonance frequency shifts (set 2)

the viscosity-temperature model, the viscosities of unknown fluids can be generated and studied.

One common aspect noticed when the figure 4.11 and figure 4.12 are compared is, the change in frequency shifts increases as the viscosity of the sucrose solution increases. Further studies is essential to understand the plots deeply which can provide various information about the fluid samples tested. Hence, the study related to effect of temperature on change in frequency shifts is incomplete.

4.7 Sensor cleaning process

In order to be able to re-use a sensor over longer periods of time, the sensor has to be efficiently cleaned. The cleaning procedure I empirically developed begins with injecting IPA in a similar manner as other samples are injected into the sensor. We see a double peak in the conductance measurement after which IPA is injected for a second time. Then, EtOH is introduced into the sensor and a similar change in the signal is observed, after which EtOH is injected again. It is followed by injecting "Helmanex" solution, a basic phosphate solution in water/IPA, once into the sensor, for which a single peak is observed. Afterwards, EtOH is injected once again, and the sensor is then flushed with water for several minutes. Figure 4.13 shows the conductance changes during sensor cleaning process. With this procedure, a sensor can be re-used for an entire set of measurements without performance loss.

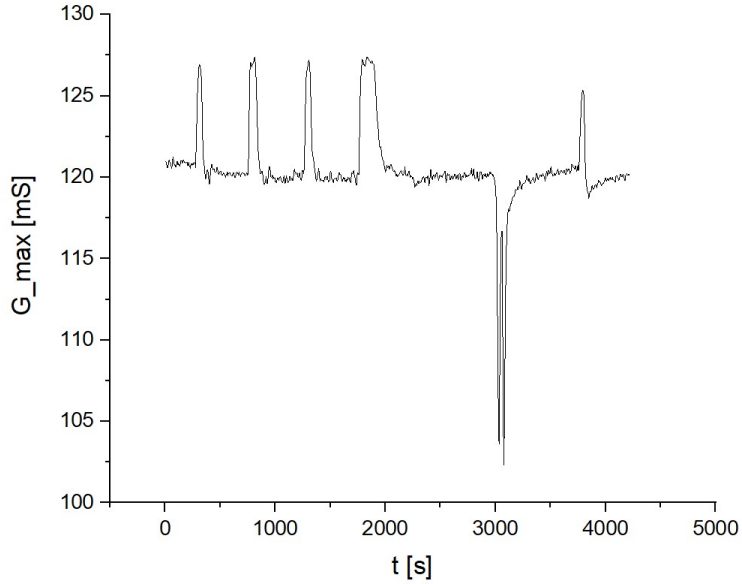

Figure 4.13: Sensor cleaning

4.8 Miscellaneous Findings

The following are observations made while conducting the measurements. These observations can be seen as indicators for problems in the experimental setup and configuration.

4.8.1 Signals measured due to the expansion and contraction of air bubbles

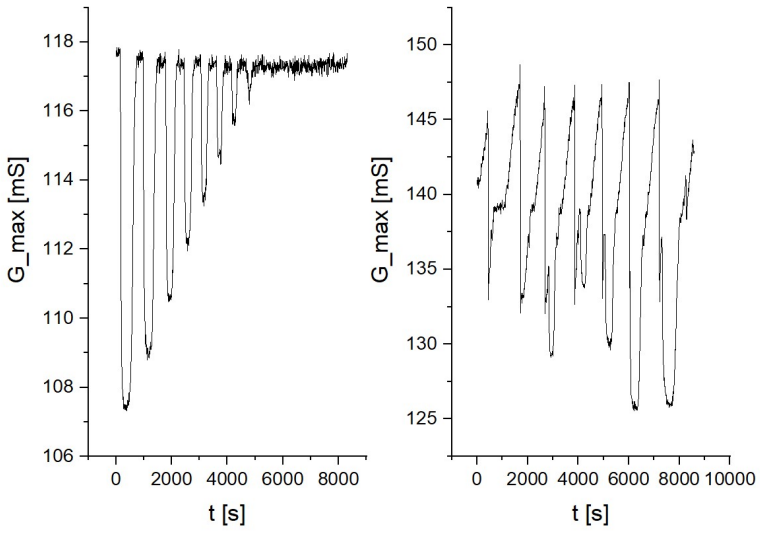

Figure 4.14: Left: Regular conductance signal for samples of various concentrations. Right: Distorted signal due to the presence of air bubbles.

Whenever a fluid sample is injected into the sensor, fluids with lower viscosity show a smaller decrease in the conductance signal measured whereas higher viscosity fluids show a larger drop in the conductance signal. This is due to the fact that the damping of acoustic waves in SAR sensor increases exponentially as the viscosity of the fluids increases.

In figure 4.14, left image shows conductance drops for sucrose solution of highest to lowest viscosities. The right image in figure 4.14 showed unexpected repetitive rise and drop of the signals despite the introduction of sucrose samples of varying viscosities. As this measurement was obtained at 35°C, the sucrose samples used were not degassed. Air dissolved in the solution was exposed to the higher temperature in a confined channel. This led to rapid formation and expansion of air bubbles, documented by the repetitive rise and drop of the signals. At 40°C, this phenomenon was quicker, which led to a repetitive zig-zag signal pattern. Hence, it is concluded that degassing of the fluid samples is essential.

4.8.2 Signal indicating a leak and causing short-circuiting

If there is a leak in the system, which causes the fluid to come in connection with the gold contact pads of the sensor and the pins touching the pads, short-circuiting occurs and an excessive response can be seen in resonance frequency vs. time plots . One example is shown in figure 4.15. The resonance frequency plots usually sees a drop in the signals and occasionally sees a slight increase of 0.1-0.3 MHz. As the measurements had been done at 40°C, the fluid evaporates over time, causing the signal stabilisation as seen in the graph.

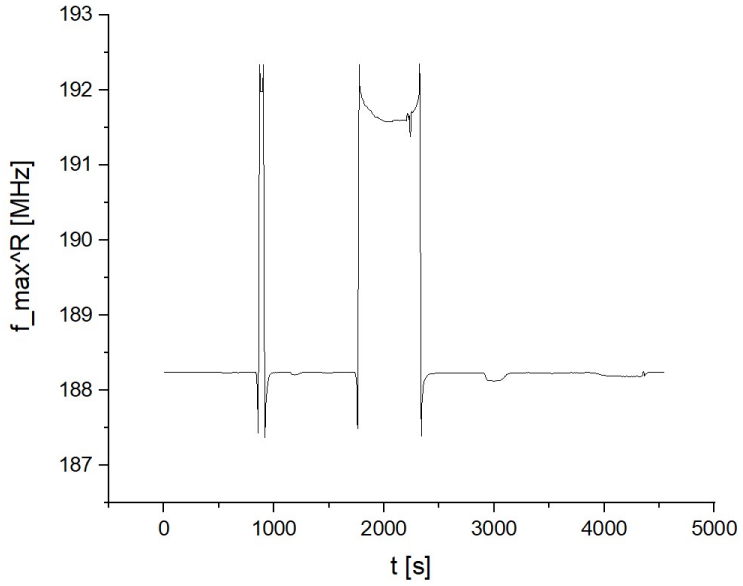

Figure 4.15: Large magnitude increase of the measured response arising from sensor short-circuiting due to a leak.

5

Conclusion and Outlook

This thesis describes the development of a new measuring platform for the earlier developed SAR/EIS tan¬dem sensor, and its use for SAR viscosity-temperature measurements. The new measurement system includes sensor holder, injection system, Mini-VNA, temperature controller, pressure pneumatic pump, sensor chip, small reagent vials, and a stand. A MATLAB script is used to interpret signals from the Mini-VNA, and is used for real-time measurement. The measuring platform successfully functions, it is compact and portable with future potential for field applications and point-of-care diagnostics. With the help of the measurement platform, elevated temperature studies can be done with the sensor. Data sets were collected, studied and analysed. The data analysis of the measurements yielded some interesting results, which can be utilized in further studies.

As a part of this thesis, a new fabrication technique has been developed for the fabrication of microfluidic sample processing chips. This technique has been successfully extended to fabrication of other microfluidic devices. Three types of sensor holders are also designed and fabricated as a part of the measurement platform, and a portable measurement setup was obtained.

This thesis is a new beginning for a new way of thinking. It stresses the importance of simplified compact and easy-to-use system modules to increase the range of potential future applications. If a successful viscosity-temperature model is established in the future, and EIS measurements are also performed in this setup, the SAR sensor can reach its full potential for studying a large number of analytical problems.

Another possibility is to develop the next iteration of the measurement platform which is completely devoid of tubes which can be quoted as 'fully integrated microfluidic platform'. This can drastically improve the flow rates in the system and thus providing a window of opportunity to study newer properties of the fluids. The designing of the fully integrated microfluidic platform, as well as the fabrication of a mold and a device holder, have in this project already been done successfully.

A desirable future improvement lies in integrating a flow rate measurement system into the existing measuring platform, which will help in accurately monitoring the flow rates, and will facilitate data analysis and quantification.

Biological samples such as lipids, proteins and blood can also be tested in the future, owing to the temperature control capabilities of the new system. SAR sensors with biomaterial coated microfluidic system can be designed to study real-time interactions of the fluids with the biomaterials.

A dry microfluidic integrated SAR sensor devoid of PDMS is possibly the next direction to explore. Photoresist materials such as SU-8 epoxy polymer are showing their potential to completely replace PDMS microfluidic devices. To this if the concept of click-chemistry is introduced for chemical surface modification, the sensor surface of the sensor can be selectively activated to detect a large variety of materials.

In summary, a new type of compact, portable measurement platform was developed with can successfully assist SAR/EIS tandem sensor measurements, for example to conduct viscosity-temperature studies with future potential as a viscosimeter for field applications and point-of-care diagnostics. The performance of the sensor setup appears to be sufficient to recommend further studies, which most likely will lead to a direct relationship between the measured parameters and the viscosity, similar to the Kanazawa-Gordon equation for QCM.

Bibliography

[1] 1995. *Expanding The Vision Of Sensor Materials.* Washington, D.C.: National Academy Press.

[2] Fraden, J., 2010. *Handbook Of Modern Sensors.* New York: Springer.

[3] Janocha, H., 2004. Actuators. Berlin: Springer.

[4] E. Iannone, Labs on Chip: Principles, Design and Technology, 1st ed. CRC Press, 10 2014.

[5] Nguyen, N., Wereley, S. and Shaegh, S., 2019. Fundamentals And Applications Of Microfluidics, 3rd ed. Artech House.

[6] Cunningham, R. and Williams, R., 1980. Diffusion In Gases And Porous Media. New York: Plenum Press.

[7] A. Manz, N. Graber, and H. Widmer, "Miniaturized total chemical analysis systems: A novel concept for chemical sensing," Sensors and Actuators B: Chemical, vol. 1, no. 1-6, pp. 244–248, jan 1990.

[8] G. M. Whitesides, "The origins and the future of microfluidics," Nature, vol. 442, no. 7101, pp. 368–373, 2006.

[9] D. E. W. Patabadige, S. Jia, J. Sibbitts, J. Sadeghi, K. Sellens, and C. T. Culbertson, "Micro total analysis systems: Fundamental advances and applications." Analytical chemistry, no. 1, p. 320, 2016.

[10] A. Rios, M. Zougagh, and M. Avila, "Review: Miniaturization through labon-a-chip: Utopia or reality for routine laboratories? a review." Analytica Chimica Acta, vol. 740, pp. 1 – 11, 2012.

[11] H. Bruus, Theoretical microfluidics., ser. Oxford master series in physics: 18 Condensed matter physics. Oxford : Oxford University Press, 2008., 2008.

[12] David J. Beebe, Glennys A. Mensing, and Glenn M. Walker. "Physics and Applications of Microfluidics in Biology". In: Annual Review of Biomedical Engineering 4.1 (2002), pp. 261–286.

[13] E. D. Daniel Royer, Elastic Waves in Solids I: Free and Guided Propagation. Springer, 2000, vol. 1.

[14] Hashimoto, K.Y., 2013. Surface Acoustic Wave Devices In Telecommunications: Modelling And Simulation. Berlin Heidelberg: Springer.

[15] Kino, G., 1987. Acoustic Waves: Devices, Imaging And Analog Signal Processing. Englewood Cliffs, N.J.: Prentice Hall PTR.

[16] Bleustein, J., 1968. A NEW SURFACE WAVE IN PIEZOELECTRIC MATERIALS. Applied Physics Letters, 13(12), pp.412-413.

[17] Love, A.E.H., 1911. Some Problems Of Geodynamics Being An Essay To Which The Adams Prize In The University Of Cambridge Was Adjudged In 1911. Cambridge: University Press.

[18] Hashimoto, K., et al., "Optimum leaky-SAW cut of LiTaO3 for minimised insertion loss devices," 1997 IEEE Ultrasonics Symposium Proceedings, Vols 1 and 2, ed. S.C. Schneider, M.Levy, and B.R. McAvoy. 1997. 245-254

[19] Caliendo, C. and Hamidullah, M., 2019. Guided acoustic wave sensors for liquid environments. Journal of Physics D: Applied Physics, 52(15), p.153001.

[20] Kustanovich, K., Yantchev, V., Doosti, B., Gözen, I. and Jesorka, A., 2019. A microfluidics-integrated impedance/surface acoustic resonance tandem sensor. Sensing and Bio-Sensing Research, 25, p.100291.

[21] Agostini, M., Greco, G. and Cecchini, M., 2018. A Rayleigh surface acoustic wave (R-SAW) resonator biosensor based on positive and negative reflectors with sub-nanomolar limit of detection. Sensors and Actuators B: Chemical, 254, pp.1-7.

[22] Assouar, M., Kirsch, P. and Alnot, P., 2009. New Love wave liquid sensor operating at 2 GHz using an integrated micro-flow channel. Measurement Science and Technology, 20(9), p.095203.

[23] Xiong, L., Chen, P. and Zhou, Q., 2014. Adhesion promotion between PDMS and glass by oxygen plasma pre-treatment. Journal of Adhesion Science and Technology, 28(11), pp.1046-1054.

[24] Maluf, N. and Williams, K., 2004. An Introduction To Microelectromechanical Systems Engineering. Boston: Artech House.

[25] K. Kustanovich, Surface acoustic wave devices for liquid-phase sensing.,ser. Licentiatuppsatser vid Institutionen för kemi och kemiteknik, Chalmers tekniska högskola: 2017:20. Göteborg : Chalmers University of Technology, 2017.

[26] Kustanovich, K., Yantchev, V., Olivefors, A., Ali Doosti, B., Lobovkina, T. and Jesorka, A., 2019. A high-performance lab-on-a-chip liquid sensor employ-

ing surface acoustic wave resonance: part II. Journal of Micromechanics and Microengineering, 29(2), p.024001.

[27] Kustanovich, K., Yantchev, V., Kirejev, V., Jeffries, G., Lobovkina, T. and Jesorka, A., 2017. A high-performance lab-on-a-chip liquid sensor employing surface acoustic wave resonance. Journal of Micromechanics and Microengineering, 27(11), p.114002.

[28] SU-8 2000 Permanent Epoxy Negative Photoresist, 4th ed., MicroChem, processing guidelines for: SU-8 2025, SU-8 2035, SU-8 2050 and SU-8 2075.

[29] Sinha, Professor G. (2017). Introduction and Classification of Sensors.

[30] Gutierrez-Osuna, Ricardo. Intelligent Sensor Systems, Wright State University.

[31] Sensors, C., 2020. Characteristics Of Sensors. [online] BrainKart. Available at: http://www.brainkart.com/article/Characteristics-of-Sensors/ [Accessed 16 June 2020].

[32] Bruus, H., 2010. Theoretical Microfluidics. Oxford: Oxford Univ. Pr.

[33] J. R. Welty, C. E. Wicks, R. E. Wilson, and G. L. Rorrer, Fundamentals of Momentum, Heat, and Mass Transfer, 5th ed. John Wiley and Sons Inc., 2008.

[34] Oliner, A., 1978. Acoustic Surface Waves. Berlin, Heidelberg: Springer Berlin Heidelberg.

[35] Saliba, JohnandDaou, Arij and Damiati, Samar and Saliba, Jessica and El-Sabban, Marwan and Mhanna, Rami. (2018). Development of Microplatforms to Mimic the In Vivo Architecture of CNS and PNS Physiology and Their Diseases. Genes. 9. 285. 10.3390/genes9060285.